Article

Molecular Cell

Structural Basis and Functional Role of Intramembrane Trimerization of the Fas/CD95 Death Receptor

Graphical Abstract

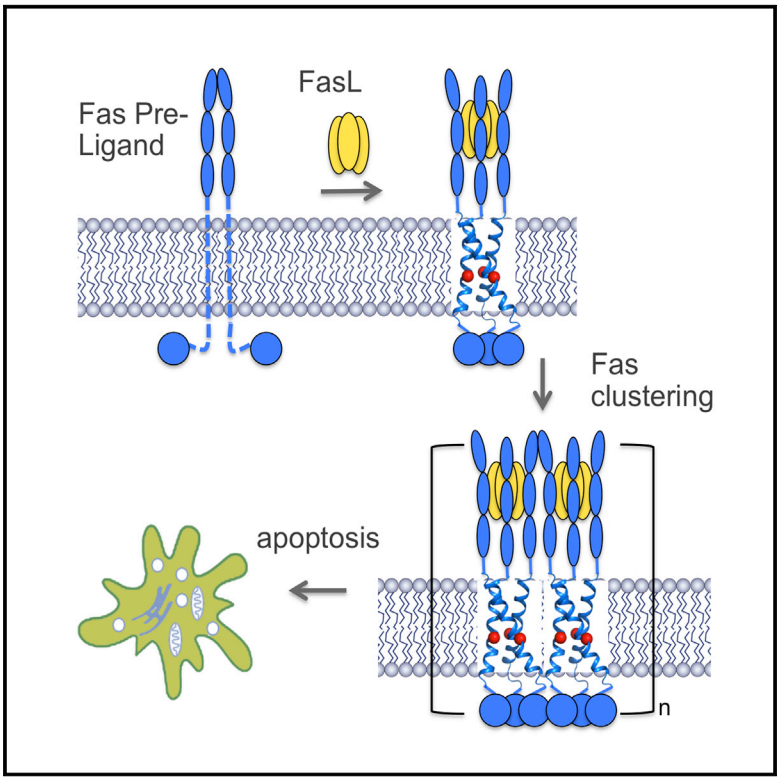

Authors

Qingshan Fu, Tian-Min Fu, Anthony C. Cruz, ..., Richard M. Siegel, Hao Wu, James J. Chou

Correspondence

wu@crystal.harvard.edu (H.W.), chou@crystal.harvard.edu (J.J.C.)

In Brief

Fas/CD95 is an apoptosis-inducing death receptor. Fu et al. determined the transmembrane domain structure of Fas and showed that the trimer assembly, which is mediated by a proline-containing motif, is essential for Fas signaling. The study provides structural explanation for several known cancer mutations in the transmembrane domain of Fas.

Highlights

- Fas transmembrane domain structures show proline-containing motif for trimerization
- The trimer conformation of the transmembrane domain is important for Fas signaling
- The trimer conformation represents signaling-active, but not pre-liganded, state of Fas
- Structural and functional data explain cancer mutations in transmembrane domain

Accession Numbers

2NA6
2NA7

Fu et al., 2016, Molecular Cell *61*, 602–613
February 18, 2016
http://dx.doi.org/10.1016/j.molcel.2016.01.009

CellPress

Molecular Cell
Article

Structural Basis and Functional Role of Intramembrane Trimerization of the Fas/CD95 Death Receptor

Qingshan Fu,[1,6] Tian-Min Fu,[1,2,6] Anthony C. Cruz,[3] Prabuddha Sengupta,[4] Stacy K. Thomas,[3] Shuqing Wang,[5] Richard M. Siegel,[3] Hao Wu,[1,2,*] and James J. Chou[1,*]

[1]Department of Biological Chemistry and Molecular Pharmacology, Harvard Medical School, Boston, MA 02115, USA
[2]Program in Cellular and Molecular Medicine, Boston Children's Hospital, Boston, MA 02115, USA
[3]Immunoregulation Section, National Institute of Arthritis and Musculoskeletal and Skin Diseases (NIAMS), NIH, Bethesda, MD 20892, USA
[4]Section on Organelle Biology, Eunice Kennedy Shriver National Institute of Child Health and Human Development, NIH, Bethesda, MD 20892, USA
[5]School of Pharmacy, Tianjin Medical University, Tianjin 300070, China
[6]Co-first author
*Correspondence: wu@crystal.harvard.edu (H.W.), chou@crystal.harvard.edu (J.J.C.)
http://dx.doi.org/10.1016/j.molcel.2016.01.009

SUMMARY

Fas (CD95, Apo-1, or TNFRSF6) is a prototypical apoptosis-inducing death receptor in the tumor necrosis factor receptor (TNFR) superfamily. While the extracellular domains of TNFRs form trimeric complexes with their ligands and the intracellular domains engage in higher-order oligomerization, the role of the transmembrane (TM) domains is unknown. We determined the NMR structures of mouse and human Fas TM domains in bicelles that mimic lipid bilayers. Surprisingly, these domains use proline motifs to create optimal packing in homotrimer assembly distinct from classical trimeric coiled-coils in solution. Cancer-associated and structure-based mutations in Fas TM disrupt trimerization in vitro and reduce apoptosis induction in vivo, indicating the essential role of intramembrane trimerization in receptor activity. Our data suggest that the structures represent the signaling-active conformation of Fas TM, which appears to be different from the pre-ligand conformation. Analysis of other TNFR sequences suggests proline-containing sequences as common motifs for receptor TM trimerization.

INTRODUCTION

Fas (CD95, Apo-1, or TNFRSF6) is a type I transmembrane (TM) protein on the cell surface and a prototypical member of the death receptor (DR) family in the tumor necrosis factor receptor (TNFR) superfamily, which also consists of TNFR1, DR3, DR4, DR5, and DR6 (Wu and Hymowitz, 2009). It is classified as a DR because of its major function as an inducer of cell death upon engagement by its ligand, Fas ligand (FasL). FasL is a type II TM protein in the TNF cytokine family (Strasser et al., 2009). The Fas/FasL system and related DRs play critical roles in mammalian biology, including maintenance of lymphocyte homeostasis, killing of pathogen-infected cells, and surveillance of cellular transformation. Thus, these receptors protect the organisms against autoimmunity and tumor development (Holland, 2014; Walczak, 2013).

Fas is composed of an N-terminal ligand-binding extracellular domain (ECD), a TM domain, and a C-terminal cytoplasmic death domain (DD). Previous studies suggest that Fas is pre-associated into non-signaling oligomers (Chan, 2000; Chan et al., 2000; Siegel et al., 2000b). Upon binding of FasL, which is trimeric in nature, Fas is induced to form signaling-competent trimers, resulting in assembly of the death-inducing signaling complex (DISC) with intracellular proteins. DISC formation begins with the recruitment of the intracellular adaptor Fas-associated DD (FADD) through DD/DD interactions. FADD also consists of a death effector domain (DED), which in turn recruits tandem DED-containing caspase-8 or caspase-10 via DED/DED interactions. It has been shown that Fas activation in cells leads to the formation of microscopically visible clusters that range from sub-micron to micron in dimensions (Kischkel et al., 1995; Siegel et al., 2004), suggesting higher-order molecular clustering.

Previous structural studies from our and other laboratories revealed a helical assembly between the DDs of Fas and FADD, with a stoichiometry of five to seven Fas molecules for five FADD molecules (Esposito et al., 2010; Wang et al., 2010). The Fas-DD/FADD-DD complex likely represents a minimal subcomplex of the DISC. In addition, DED/DED interactions have been shown to lead to the recruitment of over-stoichiometric amounts of caspases in the DISC of DRs Fas, DR4, and DR5, promoting caspase aggregation, dimerization, and auto-proteolysis (Dickens et al., 2012; Schleich et al., 2012). Since DEDs also belong to the DD fold superfamily, DED/DED interactions likely result in helical complexes and helical filaments that have been revealed for other members of the superfamily (Ferrao and Wu, 2012; Lu et al., 2014; Wu et al., 2014). The emerging model of Fas signaling is that the extracellular ligand/receptor interactions and the intracellular receptor/FADD/caspase-8 interactions cooperate to trigger large-scale clustering of the DISC and,

thus, caspase activation. The importance of the Fas pathway is further indicated by the many germline mutations of Fas in humans, which disrupt DISC formation and cause autoimmune lymphoproliferative syndrome (ALPS). These mutations map to both the ECD and the intracellular DD (Straus et al., 2001), and they are mostly heterozygous, in which the mutants dominantly interfere with the function of the wild-type (WT) Fas. Some ALPS patients also have an increased tendency to develop lymphomas (Straus et al., 2001).

The role of the Fas TM domain in pre-ligand receptor association and in Fas activation is unknown. Yet cancer-associated somatic mutations have been identified in the core of the predicted TM segment of Fas, including the C178R mutation in cutaneous squamous cell carcinoma and the L180F and P183L mutations in non-Hodgkin's lymphomas (Grønbaek et al., 1998; Lee et al., 2000), implying critical functional roles of the TM domain in signaling. For multi-pass TM proteins that convert the physical energy of ligand binding to chemical reactions across the membrane, it is well known that their TM domain conformations play important roles in the signal transduction. For most single-pass TM receptors, the role of their TM domains beyond membrane anchoring is unresolved, partly because of the following difficulty in structural studies: they are notorious for resisting crystallization and, due to their small sizes, unfeasible for visualization by cryo-electron microscopy.

The few existing single-pass TM domain structures determined using nuclear magnetic resonance (NMR) spectroscopy suggest that these domains do play specific functions. The structure of the glycophorin A TM domain revealed a GxxxG sequence motif that favors helix-helix packing in the membrane (MacKenzie et al., 1997; Russ and Engelman, 2000). Since then, a variety of TM helix dimers from different receptors have been determined (Call et al., 2006; Lau et al., 2009; Zhu et al., 2009). In the case of immunoreceptor complex, electrostatic interactions between the acidic and basic residues of the TM domains of the signaling and the receptor chains, respectively, mediate the specific assembly (Call et al., 2002, 2010). The most sophisticated roles that TMs appear to play came from studies on epidermal growth factor receptor (EGFR) and integrin, in which the dimeric TM helix bundle participates in the switching between signaling active and inactive conformations (Arkhipov et al., 2013; Endres et al., 2013; Lau et al., 2009; Mi et al., 2011; Zhu et al., 2009). However, despite the existence of many important receptors, such as those in the TNFR superfamily with trimeric ligands, there have been no reports of any TM domain structures of trimeric receptors. Nor do we know if these TMs form trimeric structures and if they are important for the signal transduction.

In this study, we reconstituted mouse and human Fas TM domains in lipid bicelles, and we used a combination of NMR spectroscopy and structure-guided mutagenesis to investigate their structure, assembly, and function. We found that the Fas TM domains formed stable trimers in lipid:detergent bicelles, but not in detergent. Structures of human and mouse Fas TM determined by NMR revealed a mode of helix-helix packing mediated by a proline-containing motif that is significantly different from classical trimeric coiled-coils in solution. These structures and structure-guided mutagenesis uncovered the molecular basis for the signaling defects of cancer-associated mutations. We found that the TM trimer is required for the signaling-competent state of liganded Fas. Analysis on the structural differences between human and mouse Fas TM domains suggested that the precise packing orientation of the triple helix bundle is critically important for trimer stability. Collectively, these data support a revised model of Fas signaling in which the specific interactions between TM helices is pivotal in cooperative formation of the DISC, in addition to trimerization at the ECD and higher-order clustering at the intracellular domain.

RESULTS

Fas TM Peptides Form Stable Homotrimers in Lipid Bilayers

We expressed the Fas TM peptides in *E. coli* as a fusion to the C terminus of the trpLE sequence with a methionine residue in between (Call et al., 2006). This methionine residue could be used as a cleavage site reacted by cyanogen bromide (CNBr) to remove the trpLE sequence. Due to the non-conserved nature of C178 in human Fas, we mutated C178 to serine, which retained trimer formation. More importantly, with the mutation we obtained superior NMR spectra that enabled high-precision structure determination in large bicelles. After cleavage with CNBr, the TM peptides were purified using high-pressure liquid-phase chromatography (Figures S1A and S1B).

Hydrophobic peptides often need to be solubilized in strong detergents and are thus not amenable to crystallization. Our approach was to reconstitute the TM domains of Fas from human and mouse (Figure 1A) into lipid:detergent bicelles and determine their structures by NMR. The lipid used was 1,2-Dimyristoyl-*sn*-Glycero-3-Phosphocholine (DMPC) and the detergent was 1,2-Dihexanoyl-*sn*-Glycero-3-Phosphocholine (DHPC). To ensure that the TM domain is embedded in a lipid bilayer environment, we used bicelles with q = 0.5 (lipid:detergent ratio of 0.5) (Figure S1C), which yields lipid discs with a diameter of ~44 Å (Sanders and Schwonek, 1992; Figure S1D).

The bicelle-reconstituted Fas TM peptides ran on SDS-PAGE as trimers (~13 kDa), whereas the peptides that were not reconstituted resolved as monomers on the gel (Figures 1B and 1C), indicating that both human and mouse Fas TMs spontaneously formed homotrimers in the lipid bilayer and that the trimeric complexes, once formed, appear to resist the strong denaturing environment of SDS-PAGE. Moreover, high chemical shift dispersion and peak homogeneity observed in the TROSY-HSQC spectra of deuterated Fas TMs in bicelles (Figures 1D and 1E) provide independent confirmation that the trimer complexes have uniform 3-fold rotational symmetry in the NMR sample.

Fas TM Structures Reveal an Unusual Mode of Helix-Helix Packing

Despite the small size of the TM peptides and the highly dispersed NMR spectra, determining the structure of the trimer faced the challenge of measuring nuclear Overhauser enhancements (NOEs) between structurally equivalent subunits having the same chemical shifts, which are required as inter-monomer distance restraints. To solve this problem, we used a mixed sample in which half of the monomers were (^{15}N/^{2}H)-labeled and the

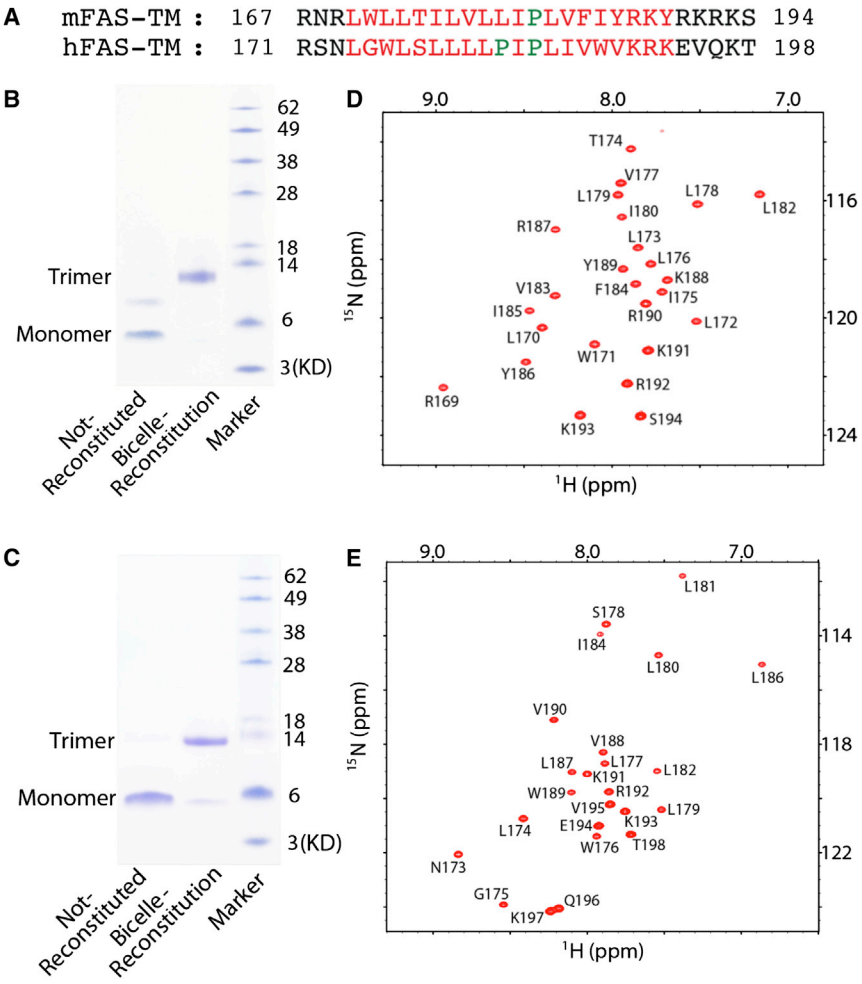

Figure 1. NMR and Biochemical Characterization of the TM Domains of Mouse and Human Fas Receptors

(A) Sequence alignment between the mouse and human Fas TM regions. The alignment is based on ClustalW2. mFAS, mouse FAS; hFAS, human FAS.

(B and C) SDS-PAGE analysis of the TM domain oligomerization in NMR sample condition for mouse (B) and human (C) Fas receptors. The gel lanes from left to right are as follows: (1) purified peptide powder dissolved in gel loading buffer; (2) purified peptide reconstituted in DMPC/DHPC bicelles (q = 0.5) as in the preparation of the NMR samples; and (3) M.W. standards. Samples were run under non-denaturing conditions.

(D and E) Two-dimensional ^{1}H-^{15}N TROSY-HSQC spectra of the TM trimers of mouse (D) and human (E) Fas receptors reconstituted in DMPC/DHPC bicelles (q = 0.5) recorded at 600 MHz. The peptides are uniformly (^{15}N, ^{13}C, ^{2}H) labeled.

other half non-deuterated to measure exclusively NOEs between the ^{15}N-attached protons of one subunit and aliphatic protons of the neighboring subunits (OuYang et al., 2013). This NOE experiment provided a sufficient number of inter-monomer NOEs (Figure S2) for deriving a unique assembly solution that has been further validated and refined using conventional NOE data. For mouse Fas TM, the 15 lowest energy structures of 75 calculated converged to root-mean-square deviation (RMSD) of ~0.829 and ~1.392 Å for backbone and all heavy atoms, respectively. For human Fas TM, the structures converged to RMSD of ~0.859 and ~1.605 Å for backbone and all heavy atoms, respectively (Figure 2A; Table 1).

Both human and mouse Fas TM trimers showed a core formed by three hydrophobic residues separated from each other by two intervening residues. These residues are Val177, Ile180, and Val183 for the mouse Fas (Figure 2B) and Leu181, Ile184, and Ile187 for the human Fas (Figure 2C). Superposition of Fas TM trimer and canonical coiled-coil trimer shows a major difference in the orientation of the three helices (Figure 2D). The regularity of these core residues led us to perform helical wheel analysis of the Fas TM trimer. In a standard coiled-coil trimer, the core is formed with residues at positions "a" and "d" of heptad repeats (Figure 2E), which is a result of the helix having 3.5 residues per helical turn. Unlike the coiled-coil helices, the hydrophobic core of the Fas TM trimer contains residues at positions "a," "d," and "g" (Figure 2F). The significant distortion from α helix is afforded by the presence of a completely conserved proline at residue positions 181 and 185 in mouse and human Fas, respectively. Indeed, both structures show a subtle kink at the proline position in the middle of the TM helix (dihedral angles are as follows: $\Phi = -64.3 \pm 5.2^{\circ}$, $\Psi = -12.9 \pm 3.8^{\circ}$ for Pro181 in mouse; $\Phi = -74.1 \pm 4.8^{\circ}$, $\Psi = -20.9 \pm 3.5^{\circ}$ for Pro185 in human). Moreover, the small proline side chain allows close van der Waals (VDW) contact with Ile180 (in mouse) or Ile184 (in human) of the adjacent monomer (Figure 2G), which results in tight packing at what appears to be the neck of the trimer. The tight packing around the proline could explain the highly stable trimeric assemblies of Fas TMs, i.e., the complexes resisted the denaturing condition of SDS-PAGE. Finally, the TM helices splay apart from the middle neck of the trimer toward both N- and C-terminal ends, where there are several positively charged residues that may associate with negatively charged lipids.

Validation of the Trimer Structures by Mutagenesis

To further understand the structure basis of trimerization of Fas TM, we examined the effects of mutations on the stability of the trimer in SDS-PAGE. Since the WT Fas TMs from both mouse and human run essentially as strong trimers in SDS-PAGE, they served as a benchmark for assembly of a stable trimer (Figure 3; Table S1). For the mouse Fas TM, a single substitution of two of the three core-forming residues, Ile180 or Val183, with alanine caused almost complete dissociation of the trimer (Figure 3B). Surprisingly, the V177A mutation in the core did not cause significant disruption, suggesting this residue position in the core could accommodate apolar groups of various sizes. As expected from the complete conservation of Pro181 in the Fas

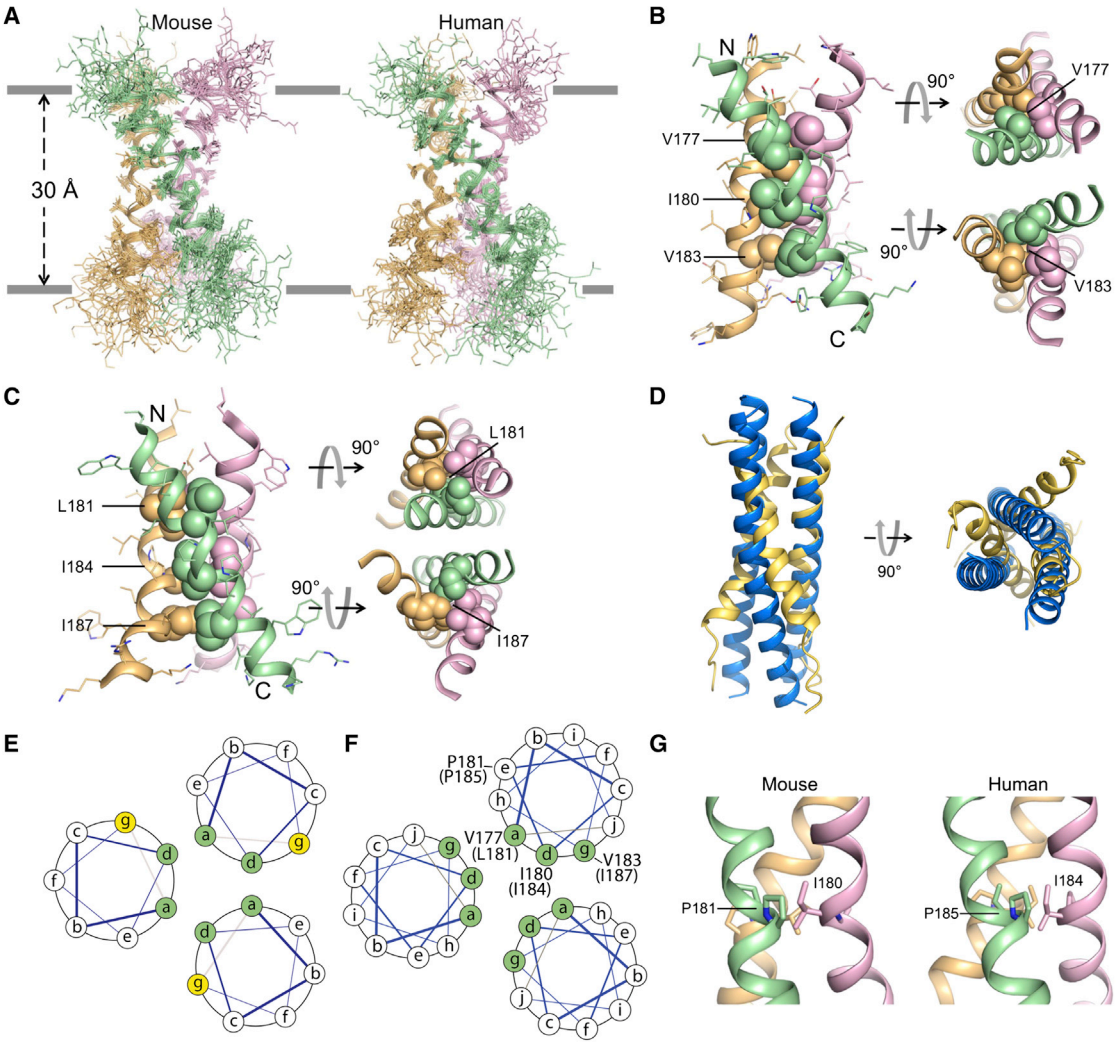

Figure 2. Structures of the Trimeric TM Domains of Fas in Bicelles

(A) Ensemble of 15 low-energy structures calculated using NMR-derived restraints. The backbone and all heavy atom RMSDs are 0.829 and 1.392 Å for mouse (left) and 0.859 and 1.605 Å for human (right). See Table 1 for more statistics.

(B) Ribbon representations of the mouse Fas TM trimers show residues that form the hydrophobic core.

(C) Ribbon representations of the human Fas TM trimers are shown.

(D) Superposition of human FAS TM trimer (yellow) and canonical coiled-coil trimer (blue, PDB: 2NVL) is shown.

(E) Helical wheel illustration of standard coiled-coil trimer showing 3.5 residues per helical turn and core positions "a" and "d" shaded in green. The positions "g" highlighted in yellow are periphery in standard coiled coil.

(F) Helical wheel illustration of Fas TM trimer shows three positions, "a," "d," and "g," involved in forming the core.

(G) Zoomed side view shows inter-helical VDW interactions between the central proline at position *i* and isoleucine at position $i - 1$.

family, mutating this residue to alanine also caused major disruption of the trimer. Another residue at the neck of the assembly is Leu182, and its mutation to alanine did not destabilize the trimer, which agrees with its position facing the lipid. Thr174 is at the interface and we found interchain NOEs between the methyl group of Thr174 and the amide of Ile175 (Figure S2C). Our results also showed that the T174A mutation did not disrupt the trimer, but the T174R mutation completely disrupted the complex, which is consistent with the structure that the small side chain of alanine should not change the interface substantially but arginine could due to its positively charged side chain.

A similar set of single mutations was tested for human Fas TM and the resulting pattern of mutational effects was essentially the same as that for mouse Fas TM (Figure 3C). The human equivalent of the mouse core-disrupting mutations, I184A and I187A, caused essentially complete dissociation of the trimer. Replacing the conserved Pro185 (Pro181 in mouse) with alanine completely disrupted the trimer. Importantly, the cancer-associated mutations C178R, L180F, and P183L (Grønbaek et al., 1998; Lee et al., 2000) were all defective in trimerization, with C178R and P183L showing more severe effects than L180F (Figure 3D). The human Fas TM, however, has an additional proline

Table 1. NMR and Refinement Statistics for FAS TM Structures

Statistics	Mouse FAS TM	Human FAS TM
NMR distance and dihedral constraints		
Distance constraints from NOE	231	243
Intra-chain NOEs	192	201
Inter-chain NOEs	39	42
Total dihedral angle restraints	120	126
ϕ (TALOS)	60	63
ψ (TALOS)	60	63
Structure[a]		
Violations (mean ± SD)		
Distance constraints (Å)	0.171 ± 0.005	0.104 ± 0.005
Dihedral angle constraints (°)	0.961 ± 0.014	0.887 ± 0.020
Deviations from idealized geometry		
Bond lengths (Å)	0.008 ± 0.000	0.007 ± 0.000
Bond angles (°)	0.898 ± 0.047	0.333 ± 0.035
Impropers (°)	0.762 ± 0.016	0.714 ± 0.030
Average pairwise RMSD (Å)[b]		
Heavy	1.392	1.605
Backbone	0.829	0.859

[a]Statistics are calculated and averaged over an ensemble of the 15 lowest energy structures of the 75 calculated structures.
[b]The precision of the atomic coordinates is defined as the average RMSD between the 15 final structures and their mean coordinates. The calculation only includes the structured regions of the protein: residues 170–189 for mouse FAS TM and residues 174–193 for human FAS TM.

at residue position 183, and mutating this proline, which is lipid facing in the structure, to leucine is as disruptive as the P185A mutation (Figure 3D). These results suggest that Pro183 in human Fas TM is also important for distorting the α helix near Pro185 to allow tight packing at the neck of the assembly (see further results below).

Prolines Provide Local Malleability for Tight Helix-Helix Assembly

Both structures in Figure 2 and single-mutation data in Figure 3 show the importance of the central proline (Pro181 in mouse and Pro185 in human) in stable trimer assembly. This is consistent with the well-recognized properties of proline as follows: (1) it allows local helix bending due to the loss of a hydrogen bond; and (2) the small size allows close VDW contact between two helices. In addition to the pivotal proline, the human Fas TM has another proline at residue position 183, and mutating it to leucine also disrupted trimerization (Figure 3D). This is unexpected because Pro183 was lipid facing in our structure (Figure 4A), and, moreover, the corresponding residue in WT mouse is a leucine (Figure 1A), which obviously did not interfere with trimerization. In an attempt to explain the strongly disruptive effect of the P183L mutation in human, which is one of the cancer-associated mutations (Grønbaek et al., 1998), we hypothesized that the additional proline in human is needed to accommodate the small differences in helix-helix packing between the human and mouse TM helix trimers. In addition to Pro183 in human, a key difference between human and mouse TM domains is that the core hydrophobic residues on two sides of the pivotal proline in human Fas, Leu181 and Ile187, are bulkier than the corresponding valines in mouse Fas (Figure 4A). Computational modeling shows that mutating Val177 and Val183 to leucine and isoleucine, respectively, causes substantial steric collision, which needs to be resolved by a wider helix-helix packing angle (Figure 4B). We thus hypothesized that the role of Pro183 in human Fas TM is to allow additional malleability near the central proline to accommodate the bigger hydrophobic cores around the neck of the trimer.

If the above hypothesis is true, then replacing the bulky Leu181 and Ile187 with valines should rescue the disruptive effect of P183L. Indeed, our mutagenesis data showed that mutating either Leu181 or Ile187 to valine in the presence of the P183L mutation partially restored trimerization and mutating both residues to valines completely restored trimerization (Figure 4C). Furthermore, we found that the P183A mutation had a disruptive effect similar to P183L. Since alanine and proline have similar sizes, the disruptive effect of P183L or P183A cannot be attributed to steric collision. Therefore, the additional proline in human Fas serves to provide the additional plasticity needed to adjust to the larger hydrophobic cores.

We also compared the calculated single-point energy change by these mutations (Table S2). For human Fas TM, the single-point energy of WT is −4.25E3 kJ/mol. The mutation P183L increases the energy to −3.98E3 kJ/mol, whereas the rescuing triple mutations P183L + L181V + I197V decrease the energy to a level even lower than that of WT (−4.55E3 kJ/mol). In the case of mouse Fas TM, the single-point energy of the WT is −4.31E3 kJ/mol. The double mutations V177L + V183I increase the energy to −3.69E3 kJ/mol, and rescuing mutations V177L + V183I + L179P decrease the energy to a level similar to that of WT (−4.23E3 kJ/mol). The above energy calculations suggest that Pro183 in human Fas TM is important for introducing the flexibility required to accommodate the hydrophobic core.

Trimerization of the TM Domain Is Essential for Spontaneous Fas-Induced Cell Death

In vitro biochemistry of human Fas mutants on the TM peptide showed that C178R, P183L, and P185A completely abolished trimerization; L180F, I184A, and I187A were partially defective; and I184V and L186A were not defective (Figure 3D). To determine if these structure-based and cancer-associated TM trimerization mutations are important for Fas signaling in the context of the full-length receptor, we examined their effects on the ability of Fas to induce cell death. We transfected HeLa cells with vector control, and WT and mutant full-length Fas constructs, and we assessed the extent of Fas expression-induced cell killing (Shatnyeva et al., 2011). Confocal microscopy confirmed that all Fas constructs localized to the cell membrane (Figure S3). At 14-hr post-transfection, cells were stained with annexin V and propidium iodide (PI). While annexin V detects externalized phosphatidylserine during the early stage of apoptosis, positive PI staining indicates loss of membrane integrity at a more advanced stage of cell death. We analyzed large populations of cells using a Cellometer automated cell counter, and we

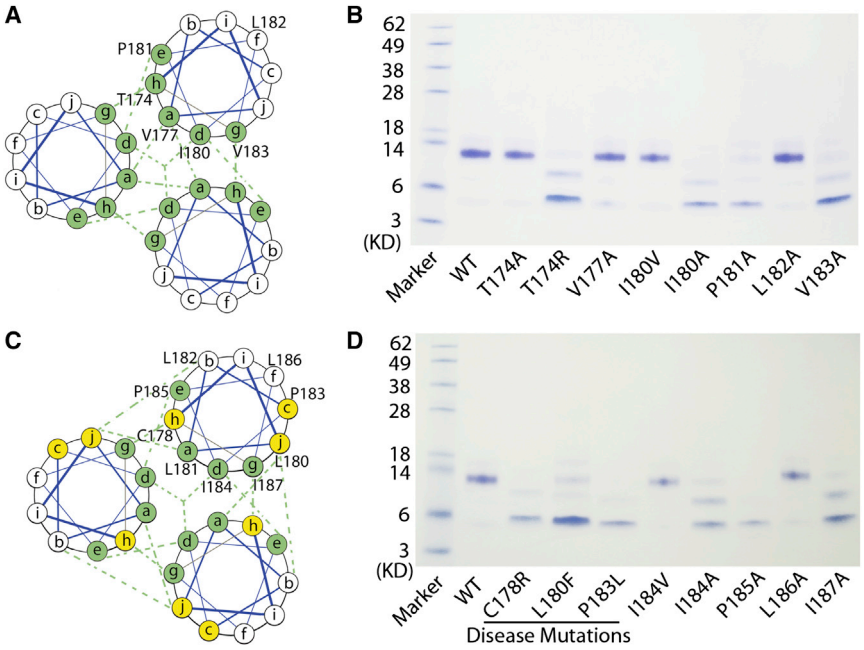

Figure 3. Effects of Single Mutations on Trimerization of the Fas TM Domains

(A) Helical wheel illustration of mouse Fas TM trimer, as in Figure 2E, showing the positions of single mutation highlighted in green. The dashed green lines indicate VDW contact between two residue positions.

(B) SDS-PAGE of bicelle-reconstituted mouse Fas TM and its mutants showing the effect of single mutations on trimerization. Samples were run under non-denaturing conditions.

(C) Helical wheel representation, as in (A), for the human Fas TM trimer shows the positions of single mutation in green as well as the disease mutation positions in yellow.

(D) SDS-PAGE of bicelle-reconstituted human Fas TM and its mutants showing the effect of single mutations on trimerization. Samples were run under non-denaturing conditions.

calculated the percentage of dead cells that were annexin V and/or PI positive.

We hypothesized that TM trimerization-defective mutants might cause reduced cell death in comparison to the WT. Of all the Fas mutants tested, C178R, P183L, and P185A were the most defective (Figure 5). C178R is a cancer-associated mutation (Lee et al., 2000) and caused trimer dissociation in vitro. As shown above, Pro183 provides the flexibility important for trimer assembly and P183L is also a cancer-causing mutant (Grønbaek et al., 1998). Pro185 is the completely conserved proline required for trimer assembly. Mutations that were either partially defective or non-defective in trimerization in vitro did not show reduced killing in these assays. Therefore, the cell death assay demonstrated that disruption of trimer assembly attenuates Fas-mediated signal transduction and cell killing. However, it appears that the Fas expression-induced cell death assay is not sufficiently sensitive to distinguish non-defective versus partially defective mutations.

Implication of the TM Trimer on Pre-ligand Receptor Assembly

The contribution of TM trimerization to Fas-induced cell death may represent either the pre- or post-liganded state of the receptor. Before ligand engagement, Fas exists in an oligomeric form stabilized by the N-terminal pre-ligand assembly domain (PLAD), which allows for efficient receptor signaling (Chan et al., 2000). To examine whether the pre-ligand assembly of Fas is affected by the TM mutants in living cells, we quantitated interactions between WT Fas molecules and those harboring mutations that disrupted in vitro trimerization of the TM domain (C178R, L180F or P183L, P183A, and P185A) using flow cytometry-based fluorescence resonance energy transfer (FRET), a technique that we have used previously to investigate self-association in Fas and other receptors in the TNFR superfamily at a single-molecule level (Lee et al., 2009; Siegel et al., 2000a, 2000b).

When cells expressing equivalent levels of the receptor proteins fused to CFP or yellow fluorescent protein (YFP) were analyzed for FRET, the mutants were all still able to associate with WT Fas to a much greater extent than a heterologous receptor TNFR1 (Figure 6A; Figure S4). The C178R mutant had the lowest interaction with WT Fas. Other than C178R, all the other mutants could not be distinguished from each other or the L186A mutant, which lies on the outside of the TM triple helix in the NMR structure. When homotypic interactions between these mutants were compared to WT Fas-Fas interactions, all the mutants were still able to self-associate, with the C178R mutant self-associating to a greater extent than WT Fas (Figure 6B). As an independent test of the effects of the TM domain on Fas pre-ligand association, we used photoactivated localization microscopy (PALM) to precisely determine the positions of single Fas molecules fused to photoactivatable GFP (PA-GFP) on the plasma membrane and to calculate the oligomerization state of individual receptor clusters (Sengupta et al., 2013). As shown in Figure 6C, 46% of WT Fas molecules were found to be in an oligomeric state, with clusters of two or three molecules representing 75% of the clusters. The P183L or L180F mutants were similar to WT Fas in their oligomerization state. Taken together, these data suggest that the Fas TM domain is not essential for pre-ligand oligomerization in the context of the full-length receptor.

Trimerization of the TM Domain Is Essential for Ligand-Induced Fas Signaling

The lack of major changes in pre-ligand receptor oligomerization due to the TM mutations suggests that the TM structure reported here may be more relevant to the conformation of the receptor after ligand engagement. To investigate this further, we tested whether TM assembly is required for cell death induced by FasL. After transfection of various forms of Fas into Fas-deficient Jurkat cells, FasL induced robust apoptosis

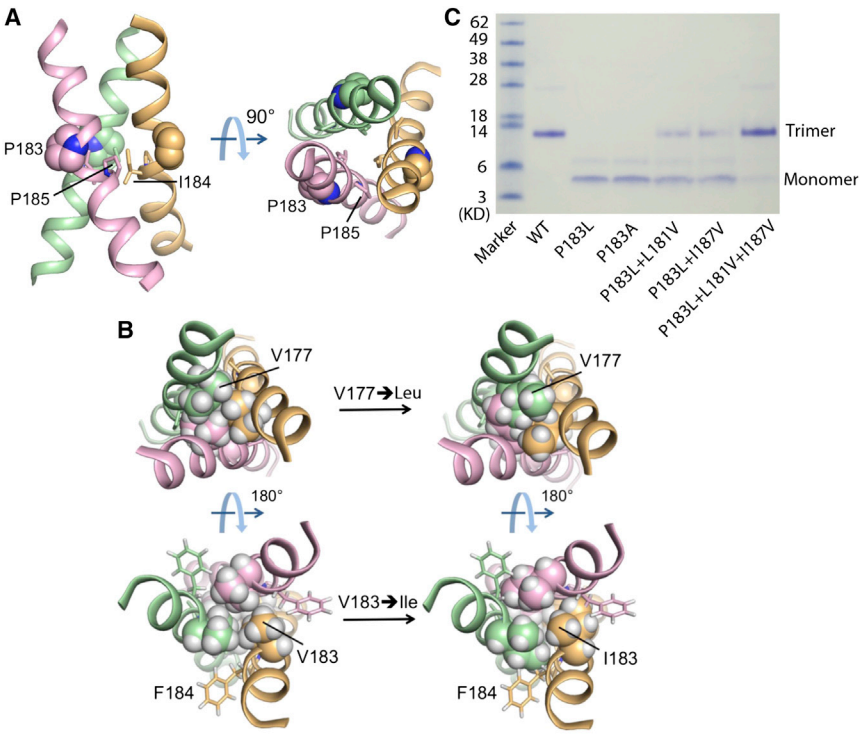

Figure 4. Role of the Lipid-Facing Proline in the Trimeric Assembly of Human Fas TM

(A) Ribbon representations of human Fas TM trimer showing the lipid-facing proline (P183) as spheres. The central proline (P185) is shown as sticks.

(B) Top and bottom views of mouse Fas TM trimer show that mutating V177 or V183 to isoleucine results in severe steric collisions on either side of the central proline.

(C) SDS-PAGE of bicelle-reconstituted human Fas TM and its mutants shows the effect of single mutations at P183 as well as compensatory mutations on trimerization.

of cells expressing WT Fas in a dose-dependent manner, while cells harboring the TM trimer-defective mutants (C178R, L180F, P183L, P183A, and P185A) were significantly resistant to FasL-induced apoptosis (Figure 6D). In Jurkat cells, receptor surface expression of YFP-positive cells as determined by anti-Fas antibody staining was decreased for TM mutants, particularly C178R, which also was reflected in FasL binding (Figure S5). It is likely that the introduction of a positive charge made the C178R mutant less stable on the membrane surface, which may further contribute to its pathogenicity. The L186A mutant, which is not in the trimer interface, mediated an intermediate amount of cell death slightly less than the WT receptor, perhaps reflecting a contribution of this residue to interactions between receptor trimers, which are likely to occur given the larger oligomeric structures triggered by receptor ligation and required for apoptosis (Siegel et al., 2004, Wang et al., 2010). TM domain mutations did not disrupt cell death as much as a DD mutant (A257D) found in ALPS patients, which disrupts the type III interface stabilizing the Fas/FADD-signaling complex and functions as a dominant-negative mutation in ALPS (Wang et al., 2010). Collectively, the destabilizing effect of mutations on TM trimerization may affect Fas signaling at multiple levels, including surface receptor expression and formation of a productive apoptosis-inducing signaling complex.

Since the ability of DD-deleted or -mutated Fas to interfere with WT Fas signaling depends on the assembly of these mutants into receptor trimers upon signaling (Siegel et al., 2000b), Fas TM mutants may exhibit reduced ability to interfere with Fas-induced apoptosis. To test whether this is the case, we co-transfected DD-deleted (ΔDD) versions of each of these three TM mutants with WT Fas and induced apoptosis with FasL. As expected, Fas ΔDD strongly inhibited the ability of WT Fas to induce apoptosis (Figure 6E). However, Fas TM domain mutations significantly reduced the ability of the Fas ΔDD construct to block cell death induced by WT Fas. The reduced ability to interfere with WT Fas signaling is consistent with the loss of heterozygosity of these mutants at the Fas locus in cancer cells (Grønbaek et al., 1998; Lee et al., 2000), in contrast to the DD mutations in ALPS, which are co-expressed with WT receptors (Straus et al., 2001).

DISCUSSION

Proline-Containing Sequence Motif for Trimeric TM Assembly

Our studies demonstrated that the TM domains of Fas form stable trimers in lipid bilayer, suggesting that these TM sequences possess intrinsic propensities to trimerize. This is in line with the ligand-induced trimerization of the receptor ECD. The NMR structures of the TM trimers revealed a mode of TM helix assembly in which prolines play critical roles in providing optimal bending angles and local plasticity to allow close helix-helix packing. This trimeric structure is important for the ability of Fas to induce cell death, explaining the disease phenotypes of Fas TM mutations. The mode of Fas TM assembly is entirely different from TM helix dimers formed around the GxxxG sequence motif (Russ and Engelman, 2000), the more common coiled-coil assembly of TM helices that form higher-order oligomers (Oxenoid and Chou, 2005; Rout et al., 2014; Wang et al., 2009), and the relatively non-specific, cation-mediated trimeric and tetrameric intermediates of the DAP12 TM domain (Knoblich et al., 2015). The unique structural feature implies the existence of a sequence determinant for the trimeric assembly of Fas TM.

By comparing the structures of the mouse and human Fas TM trimers and their corresponding patterns of mutational effects, we can make the following conclusions about the structural elements essential for trimerization. First, the conserved Pro181 in mouse and Pro185 in human, denoted here as P(*i*), introduce

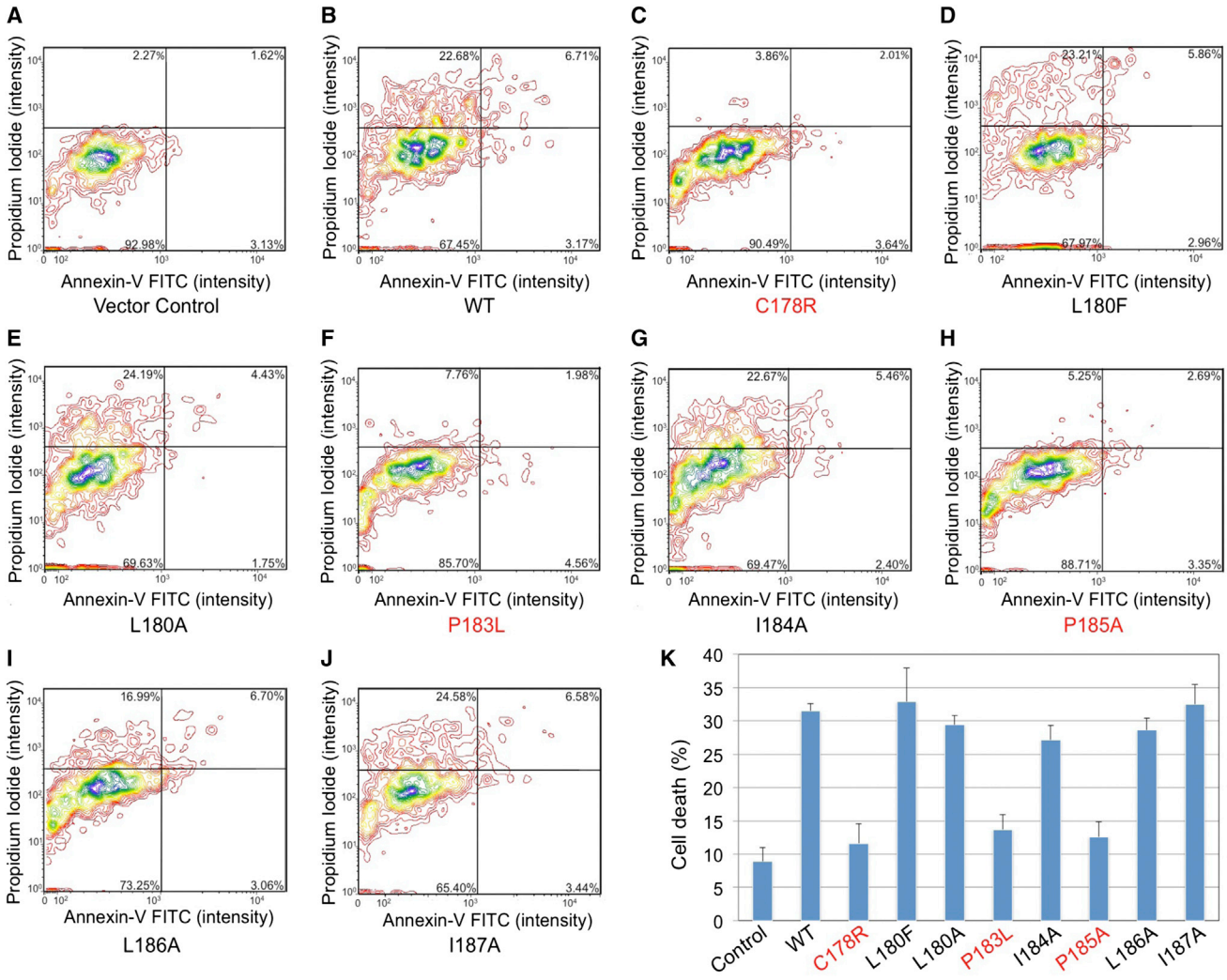

Figure 5. Trimerization of the TM Domain Is Essential for Overexpression-Induced Fas Killing

(A–J) HeLa cells transiently overexpressed with WT and mutant Fas were stained by PI and annexin V and analyzed by Cellometer. One representative dataset of three is shown. High PI- and/or high annexin V-stained cells were considered dead cells.

(K) Plotted cell death ratios in WT and mutant Fas-overexpressed HeLa cells. The data show that C178R, P183L, and P185A mutant Fas were partially defective in cell killing compared to WT Fas. Error bars are derived from three independent experiments.

local bending of the backbone structure that allows close helix-helix packing around this residue. Second, the hydrophobic residue preceding P(i), denoted here as $\Phi(i-1)$, packs closely against P(i) of the adjacent monomer. The $\Phi(i-1)$ residue also forms the hydrophobic core at position $i-1$. Third, the hydrophobic residue at position $i + 2$, denoted here as $\Phi(i + 2)$, forms the hydrophobic core at position $i + 2$. These three residues have been shown by mutagenesis to be important for assembly. The residue at position $i + 1$ (denoted as x) is lipid facing and its mutation does not affect trimerization. Therefore, the sequence motif that determines trimerization of Fas TM appears to be ΦPxΦ, where Φ represents hydrophobic residues such as leucine, isoleucine, or valine; P is proline; and x can be any residues that can partition in the lipid environment, except for proline and glycine.

We found that the ΦPxΦ sequence is present in the TM domains of other families of the TNFR superfamily, including TNFR1, DR3, and DR6, although the positions of the sequence motif in the membrane vary (Figure 7A). It is, therefore, likely that the Fas TM structures represent a structural archetype for many members of the TNFR superfamily.

Role of Intramembrane Trimerization in Fas Signaling

Based on the Fas TM trimer structures, we have identified several mutations that disrupt trimerization, including those reported to be associated with cancer (Grønbaek et al., 1998; Lee et al., 2000). The reduced spontaneous or FasL-induced apoptosis in cells expressing Fas with these mutations indicates that the TM trimer structure is required for receptor function. Our observations using FRET and super-resolution microscopy that

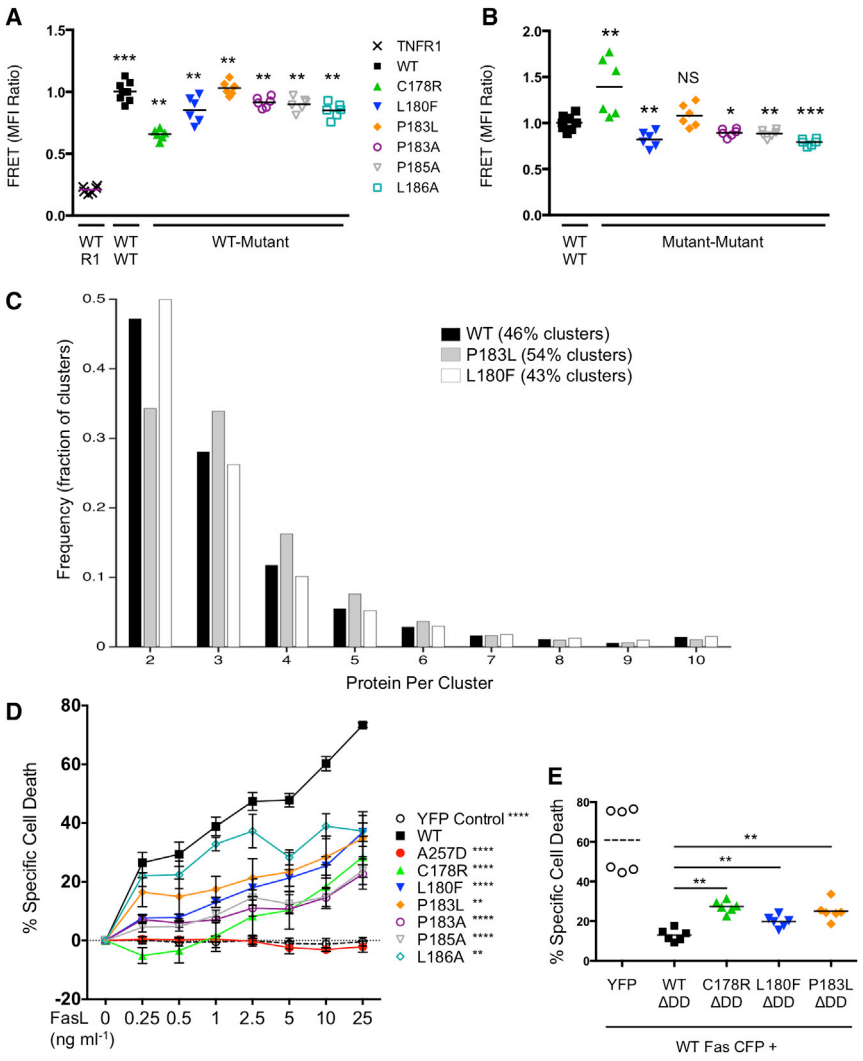

Figure 6. Effects of Fas TM Domain Mutants on Receptor Pre-association and FasL-Induced Apoptosis

(A and B) Relative FRET between the indicated CFP and YFP fusion proteins of Fas in transfected 293T cells. The fold change in FRET relative to WT-WT interactions for heterotypic mutant:WT (A) and homotypic (B) interactions are shown. Data are from two independent experiments, with each repeat shown as one point, and are representative of five independent experiments. Statistical comparisons to WTFas-TNFR1 association (A) and WTFas self-association (B) are shown (*$p \leq 0.05$, **$p \leq 0.01$, and ***$p \leq 0.001$ by Mann-Whitney).

(C) Oligomerization state of WT, P183L, and L180F Fas mutants on the plasma membrane of COS-7 assessed by quantitative analysis of PALM datasets. The spatial distribution of single PAGFP-tagged CD95, CD95-P183L, and CD95-L180F across the plasma membrane was analyzed by Hoshen-Kopelman-based algorithm to identify individual protein clusters, and the number of proteins within each identified cluster was counted. The plot shows the frequency of occurrence of clusters containing specified number of proteins, and the percentage of clustered molecules are shown in the legend.

(D) Fas-deficient Jurkat RapoC2 cells were transfected with either WT Fas or the indicated TM mutation and stimulated with increasing amounts of FasL-LZ for 18 hr to induce apoptosis. Data shown are cumulative of three independent experiments, each performed in triplicate, represented as mean ± SEM. Unpaired t test was used for statistical analyses (**$p \leq 0.01$ and ****$p \leq 0.0001$ for all concentrations above 2.5 ng ml^{-1} of the indicated mutant compared to WT).

(E) Dominant-negative interference assay with DD-truncated (ΔDD) Fas-YFP fusion constructs co-transfected with full-length Fas-CFP fusion constructs into Jurkat RapoC2 cells. Transfected cells were stimulated with 25 ng/ml FasL-LZ for 18 hr and CFP^+YFP^+ cells of equivalent relative fluorescence were assessed for cell death. Asterisks represent significance ($p < 0.005$) for comparison of the ability of mutant Fas constructs to confer resistance to FasL-induced apoptosis compared with the WT ΔDD protein. Data are cumulative of two independent experiments, each performed in triplicate.

the same disruptive mutations did not decrease interactions between the mutant receptor chains in the absence of FasL suggests that the principal function of the TM domain is to stabilize the liganded state of the receptor, rather than pre-ligand association, which is the function of the N-terminal PLAD (Siegel et al., 2000b). Whether the pre-ligand association state of Fas is trimeric or dimeric has been a matter of debate. The lack of interference with pre-ligand association by the TM mutants defective in trimerization may support a dimer state observed in the crystal structure of ECD of TNFR1 (Naismith et al., 1995). The super-resolution microscopy data showing that monomers, dimers, and trimers of receptors co-exist on the plasma membrane before ligation suggest that the pre-ligand state may be more of a dynamic equilibrium among oligomeric states. Although the TM domain does not interact with the ligand, it may help in stabilizing the ligand-bound state of Fas and, in turn, facilitate the oligomerization that is necessary for efficient recruitment and activation of caspase-8, which is critical for initiating the apoptotic caspase cascade. The reduced ability of a DD-truncated version of Fas to interfere with WT Fas signaling when mutations are introduced into the TM domain (Figure 6E) supports a functional role for the TM domain in oligomerizing Fas during ligand-induced signaling.

Explanation of Cancer-Associated Fas TM Mutations

Somatic mutations in the human Fas TM domain are associated with malignancy, with the L180F and P183L mutations associated with lymphoma and the C178R mutation with squamous cell carcinoma (Grønbaek et al., 1998; Lee et al., 2000). Our SDS-PAGE results show that all three mutations have strong disruptive effects on TM domain trimerization (Figure 3D). The side chain of Cys178 is located at the interface of helices (Figure 3C) and its mutation to the much larger arginine should result in major steric collisions. Moreover, placing three positively charged arginines in the narrow diamagnetic space is expected

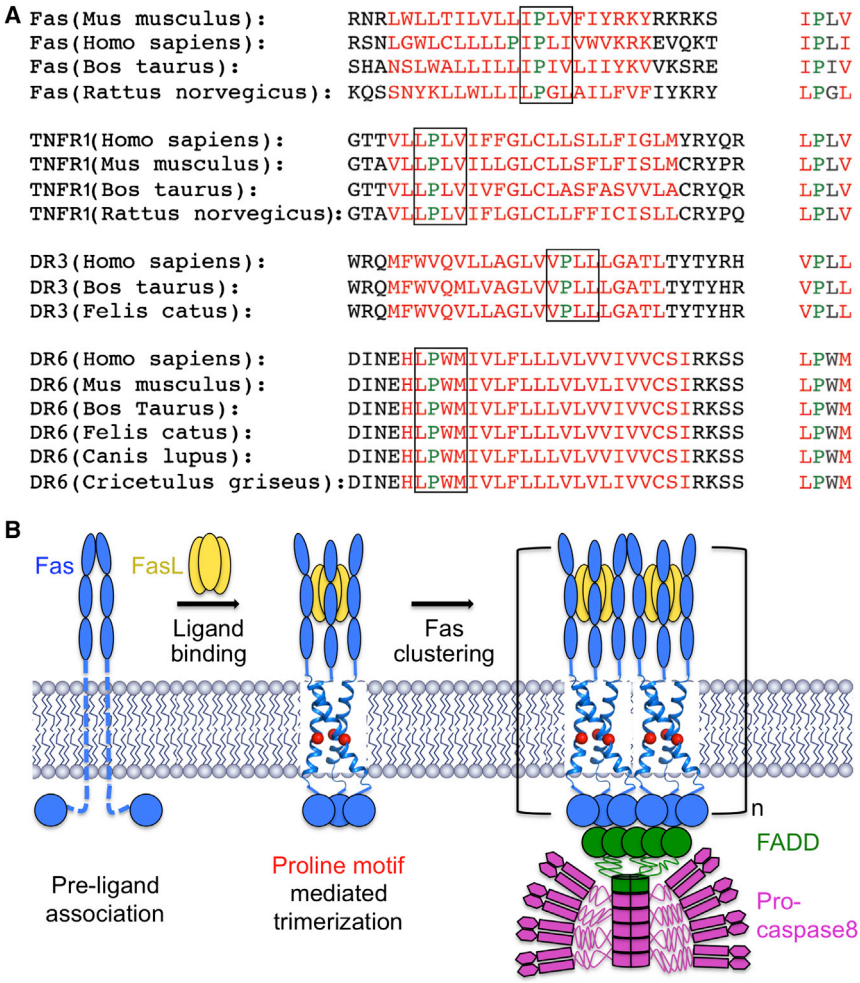

Figure 7. Implication of Fas TM Trimerization to TM Signaling by TNFRs

(A) TM domain sequences within different receptor families of the TNFR superfamily, aligned using the ΦPxΦ motif, are shown.

(B) Schematic illustration of the role of proline motif-mediated Fas TM trimerization in stabilizing the trimeric receptor conformation that is signaling active. Dimeric pre-ligand association is supported by this study and observations of crystallographic dimers in the unliganded ECD of TNFR1 (Naismith et al., 1995). Higher-order clustering of liganded Fas is supported by structural and functional studies of intracellular interactions.

to introduce strong repulsive and disruptive forces. Leu180 is also at the helix-helix interface (Figure 3C); its side chain inserts between Leu181 and Pro185 of the adjacent TM helix, forming optimal inter-helical VDW contacts. Mutating Leu180 to phenylalanine, which has different shape and electronic properties, is expected to have destabilization effect at this position. Pro183 is lipid facing in the structure (Figure 4A). As demonstrated above, the P183L mutation reduces the flexibility near the central core of the trimer required for optimal packing of the core residues and, as a result, also disrupts the trimer assembly (Figure 3D).

Unlike mutations in the DD, which can inhibit the function of the WT receptor, the TM Fas mutations in cancer are associated with loss of heterozygosity, with deletions in the other allele of Fas. The reduced ability of these mutants to promote apoptosis shows that disrupting intramembrane trimerization of the receptor during signaling is the likely molecular explanation for these disease-associated mutations. Interfering with or stabilizing the TM domain of Fas would be a novel strategy for therapeutic manipulation of the Fas pathway.

Conclusions

In summary, this study demonstrates that the TM domains of the Fas receptors form stable homotrimers in lipid bilayer, and the stability of trimer assembly is important for the ability of the receptors to signal. The structures of the Fas TM trimers represent a mode of TM helix assembly in which the prolines play the critical role of providing local plasticity for allowing close helix-helix packing in the middle of the TM domains. Based on the presence of conserved prolines in the predicted TM segments of other TNFR families, the reported trimer structure may represent a structural archetype for the rest of the TNFR superfamily, as well as other receptor systems that trimerize.

Our functional data, both from in vivo and in vitro experiments, unequivocally show that the structure of the trimeric TM complex plays an important role in supporting the signaling active state of the receptor by stabilizing the ligand-bound state of the Fas ECD and the oligomeric arrangement necessary for downstream recruitment of caspases (Figure 7B). Furthermore, we provide evidence to show that the reported TM trimer structure is not relevant to the TM domain conformation of the pre-ligand receptor complex. Altogether, our findings provide a molecular explanation for the known cancer-causing Fas TM mutations as all of them disrupt the reported TM trimer structure and, consequently, reduce the ability of the mutant receptors to properly assemble and signal.

EXPERIMENTAL PROCEDURES

Protein Production and Reconstitution

The human Fas TM RSNLGWLSLLLLPIPLIVWVKRKEVQKT and the mouse Fas TM RNRLWLLTILVLLIPLVFIYRKYRKRKS were expressed and purified using protocols similar to those developed previously (Call et al., 2006; Schnell and Chou, 2008).

Structure Calculation

The monomer structure was first determined using intramonomer NOE restraints and backbone dihedral restraints derived from chemical shifts. Three copies of the monomer structure were used to construct an initial model of the trimer using inter-monomer NOE restraints. For each inter-monomer restraint between two adjacent monomers, three identical distance restraints were assigned respectively to all pairs of neighboring monomers to satisfy the

condition of 3-fold rotational symmetry. Finally, the trimer was refined against the complete set of NOE restraints (including intra-monomer and inter-monomer distance restraints) and dihedral restraints. A total of 75 structures were calculated and 15 low-energy structures were selected as the structural ensemble. Restraint and refinement statistics are shown in Table 1 (Supplemental Experimental Procedures).

Fas Ligand Preparation

FasL-LZ was prepared as previously described (A.C.C., P.S., S.K.T., and R.M.S., unpublished data; Ramaswamy et al., 2011). Briefly, the ECD of FasL was fused to a FLAG tag and an isoleucine zipper motif to allow self-assembly. HEK293T cells were transfected with the FasL construct for overexpression, with cell supernatants collected and purified over anti-FLAG magnetic beads (anti-FLAG M2 magnetic beads, Sigma). Quantitation was performed by ELISA (R&D Systems).

FRET

Full-length (amino acid [aa] 1–317) or DD-truncated (aa 1–210) human Fas was cloned into pECFP-N1 or pEYFP-N1 (Clontech Laboratories), modified to express an N-terminal hemagglutinin (HA) tag and utilize the TNFR2 leader sequence for efficient surface expression. TM mutations were introduced into the constructs by site-directed mutagenesis. After confirmation of both sequence and expression, 2 μg of each construct was transfected into 293T cells. Then, 48 hr after transfection, flow cytometric detection of FRET intensity was performed (Siegel et al., 2000a, 2000b) using a SORP LSRII Fortessa (BD Biosciences) with 447/488 nm dual-laser excitation. Constructs expressing either full-length TNFR1 p60 or TACI with C-terminal CFP or YFP fusion were used as controls.

PALM

PAGFP-labeled WT, P183L, and L180F Fas constructs (CD95-PAGFP, CD95-P183L-PAGFP, and CD95-L180F-PAGFP, respectively) were transiently transfected into COS-7 cells using Fugene 6 (Promega). Cells were fixed with 4% paraformaldehyde and 0.2% glutaraldehyde in PBS 20–24 hr post-transfection and imaged by PALM to precisely localize the positions of single PAGFP-labeled protein molecules. Next, a composite super-resolution image was generated by combining all the single-molecule positions identified in the entire set of image frames of a PALM time-series experiment. The composite image was analyzed using Hoshen-Kopelman algorithm to identify and spatially localize individual clusters of CD95/CD95-P183L/CD95-L180F molecules.

ACCESSION NUMBERS

The accession numbers for the structure coordinate and structural constraints of mouse and human Fas TM domains reported in this paper are PDB: 2NA6 and 2NA7, respectively. The accession numbers for the chemical shift values of mouse and human Fas TM domains reported in this paper are Biological Magnetic Resonance Data Bank (BMRB): 25929 and 25930, respectively.

SUPPLEMENTAL INFORMATION

Supplemental Information includes Supplemental Experimental Procedures, five figures, and two tables and can be found with this article online at http://dx.doi.org/10.1016/j.molcel.2016.01.009.

AUTHOR CONTRIBUTIONS

H.W., J.J.C., R.M.S., Q.F., and T.-M.F. conceived of the study. Q.F. and T.-M.F. prepared samples for structural and in vitro assembly measurements. Q.F. and J.J.C. collected and analyzed NMR data and determined the structures. T.-M.F. and H.W. performed and analyzed expression-induced apoptosis assays. A.C.C., S.K.T., P.S., and R.M.S. performed and analyzed ligand-induced and ligand-free receptor-signaling and assembly assays. S.W. performed all computational modeling analyses. J.J.C., H.W., and R.M.S. wrote the paper and all authors contributed to editing of the manuscript.

ACKNOWLEDGMENTS

The NMR data were collected at MIT-Harvard CMR (supported by NIH grant P41 EB-002026). We thank the NIAMS Flow Cytometry Core for technical assistance. This work was supported by NIH grants HL103526 to J.J.C. and AI050872 to H.W. and by NIH NIAMS intramural research program and project grant Z01-AR041133 to R.M.S. We would like to thank Timothy Springer for the insightful discussion.

Received: August 22, 2015
Revised: November 17, 2015
Accepted: January 4, 2016
Published: February 4, 2016

REFERENCES

Arkhipov, A., Shan, Y., Das, R., Endres, N.F., Eastwood, M.P., Wemmer, D.E., Kuriyan, J., and Shaw, D.E. (2013). Architecture and membrane interactions of the EGF receptor. Cell *152*, 557–569.

Call, M.E., Pyrdol, J., Wiedmann, M., and Wucherpfennig, K.W. (2002). The organizing principle in the formation of the T cell receptor-CD3 complex. Cell *111*, 967–979.

Call, M.E., Schnell, J.R., Xu, C., Lutz, R.A., Chou, J.J., and Wucherpfennig, K.W. (2006). The structure of the zetazeta transmembrane dimer reveals features essential for its assembly with the T cell receptor. Cell *127*, 355–368.

Call, M.E., Wucherpfennig, K.W., and Chou, J.J. (2010). The structural basis for intramembrane assembly of an activating immunoreceptor complex. Nat. Immunol. *11*, 1023–1029.

Chan, F.K. (2000). The pre-ligand binding assembly domain: a potential target of inhibition of tumour necrosis factor receptor function. Ann. Rheum. Dis. *59* (*Suppl 1*), i50–i53.

Chan, F.K.M., Chun, H.J., Zheng, L., Siegel, R.M., Bui, K.L., and Lenardo, M.J. (2000). A domain in TNF receptors that mediates ligand-independent receptor assembly and signaling. Science *288*, 2351–2354.

Dickens, L.S., Boyd, R.S., Jukes-Jones, R., Hughes, M.A., Robinson, G.L., Fairall, L., Schwabe, J.W., Cain, K., and Macfarlane, M. (2012). A death effector domain chain DISC model reveals a crucial role for caspase-8 chain assembly in mediating apoptotic cell death. Mol. Cell *47*, 291–305.

Endres, N.F., Das, R., Smith, A.W., Arkhipov, A., Kovacs, E., Huang, Y., Pelton, J.G., Shan, Y., Shaw, D.E., Wemmer, D.E., et al. (2013). Conformational coupling across the plasma membrane in activation of the EGF receptor. Cell *152*, 543–556.

Esposito, D., Sankar, A., Morgner, N., Robinson, C.V., Rittinger, K., and Driscoll, P.C. (2010). Solution NMR investigation of the CD95/FADD homotypic death domain complex suggests lack of engagement of the CD95 C terminus. Structure *18*, 1378–1390.

Ferrao, R., and Wu, H. (2012). Helical assembly in the death domain (DD) superfamily. Curr. Opin. Struct. Biol. *22*, 241–247.

Grønbaek, K., Straten, P.T., Ralfkiaer, E., Ahrenkiel, V., Andersen, M.K., Hansen, N.E., Zeuthen, J., Hou-Jensen, K., and Guldberg, P. (1998). Somatic Fas mutations in non-Hodgkin's lymphoma: association with extranodal disease and autoimmunity. Blood *92*, 3018–3024.

Holland, P.M. (2014). Death receptor agonist therapies for cancer, which is the right TRAIL? Cytokine Growth Factor Rev. *25*, 185–193.

Kischkel, F.C., Hellbardt, S., Behrmann, I., Germer, M., Pawlita, M., Krammer, P.H., and Peter, M.E. (1995). Cytotoxicity-dependent APO-1 (Fas/CD95)-associated proteins form a death-inducing signaling complex (DISC) with the receptor. EMBO J. *14*, 5579–5588.

Knoblich, K., Park, S., Lutfi, M., van 't Hag, L., Conn, C.E., Seabrook, S.A., Newman, J., Czabotar, P.E., Im, W., Call, M.E., and Call, M.J. (2015). Transmembrane Complexes of DAP12 Crystallized in Lipid Membranes Provide Insights into Control of Oligomerization in Immunoreceptor Assembly. Cell Rep. *11*, 1184–1192.

Lau, T.L., Kim, C., Ginsberg, M.H., and Ulmer, T.S. (2009). The structure of the integrin alphaIIbbeta3 transmembrane complex explains integrin transmembrane signalling. EMBO J. *28*, 1351–1361.

Lee, S.H., Shin, M.S., Kim, H.S., Park, W.S., Kim, S.Y., Jang, J.J., Rhim, K.J., Jang, J., Lee, H.K., Park, J.Y., et al. (2000). Somatic mutations of Fas (Apo-1/CD95) gene in cutaneous squamous cell carcinoma arising from a burn scar. J. Invest. Dermatol. *114*, 122–126.

Lee, J.J., Rauter, I., Garibyan, L., Ozcan, E., Sannikova, T., Dillon, S.R., Cruz, A.C., Siegel, R.M., Bram, R., Jabara, H., and Geha, R.S. (2009). The murine equivalent of the A181E TACI mutation associated with common variable immunodeficiency severely impairs B-cell function. Blood *114*, 2254–2262.

Lu, A., Kabaleeswaran, V., Fu, T., Magupalli, V.G., and Wu, H. (2014). Crystal structure of the F27G AIM2 PYD mutant and similarities of its self-association to DED/DED interactions. J. Mol. Biol. *426*, 1420–1427.

MacKenzie, K.R., Prestegard, J.H., and Engelman, D.M. (1997). A transmembrane helix dimer: structure and implications. Science *276*, 131–133.

Mi, L.Z., Lu, C., Li, Z., Nishida, N., Walz, T., and Springer, T.A. (2011). Simultaneous visualization of the extracellular and cytoplasmic domains of the epidermal growth factor receptor. Nat. Struct. Mol. Biol. *18*, 984–989.

Naismith, J.H., Devine, T.Q., Brandhuber, B.J., and Sprang, S.R. (1995). Crystallographic evidence for dimerization of unliganded tumor necrosis factor receptor. J. Biol. Chem. *270*, 13303–13307.

OuYang, B., Xie, S., Berardi, M.J., Zhao, X., Dev, J., Yu, W., Sun, B., and Chou, J.J. (2013). Unusual architecture of the p7 channel from hepatitis C virus. Nature *498*, 521–525.

Oxenoid, K., and Chou, J.J. (2005). The structure of phospholamban pentamer reveals a channel-like architecture in membranes. Proc. Natl. Acad. Sci. USA *102*, 10870–10875.

Ramaswamy, M., Cruz, A.C., Cleland, S.Y., Deng, M., Price, S., Rao, V.K., and Siegel, R.M. (2011). Specific elimination of effector memory CD4+ T cells due to enhanced Fas signaling complex formation and association with lipid raft microdomains. Cell Death Differ. *18*, 712–720.

Rout, A.K., Strub, M.P., Piszczek, G., and Tjandra, N. (2014). Structure of transmembrane domain of lysosome-associated membrane protein type 2a (LAMP-2A) reveals key features for substrate specificity in chaperone-mediated autophagy. J. Biol. Chem. *289*, 35111–35123.

Russ, W.P., and Engelman, D.M. (2000). The GxxxG motif: a framework for transmembrane helix-helix association. J. Mol. Biol. *296*, 911–919.

Sanders, C.R., 2nd, and Schwonek, J.P. (1992). Characterization of magnetically orientable bilayers in mixtures of dihexanoylphosphatidylcholine and dimyristoylphosphatidylcholine by solid-state NMR. Biochemistry *31*, 8898–8905.

Schleich, K., Warnken, U., Fricker, N., Oztürk, S., Richter, P., Kammerer, K., Schnölzer, M., Krammer, P.H., and Lavrik, I.N. (2012). Stoichiometry of the CD95 death-inducing signaling complex: experimental and modeling evidence for a death effector domain chain model. Mol. Cell *47*, 306–319.

Schnell, J.R., and Chou, J.J. (2008). Structure and mechanism of the M2 proton channel of influenza A virus. Nature *451*, 591–595.

Sengupta, P., Jovanovic-Talisman, T., and Lippincott-Schwartz, J. (2013). Quantifying spatial organization in point-localization superresolution images using pair correlation analysis. Nat. Protoc. *8*, 345–354.

Shatnyeva, O.M., Kubarenko, A.V., Weber, C.E., Pappa, A., Schwartz-Albiez, R., Weber, A.N., Krammer, P.H., and Lavrik, I.N. (2011). Modulation of the CD95-induced apoptosis: the role of CD95 N-glycosylation. PLoS ONE *6*, e19927.

Siegel, R.M., Chan, F.K., Zacharias, D.A., Swofford, R., Holmes, K.L., Tsien, R.Y., and Lenardo, M.J. (2000a). Measurement of molecular interactions in living cells by fluorescence resonance energy transfer between variants of the green fluorescent protein. Sci. STKE *2000*, pl1.

Siegel, R.M., Frederiksen, J.K., Zacharias, D.A., Chan, F.K., Johnson, M., Lynch, D., Tsien, R.Y., and Lenardo, M.J. (2000b). Fas preassociation required for apoptosis signaling and dominant inhibition by pathogenic mutations. Science *288*, 2354–2357.

Siegel, R.M., Muppidi, J.R., Sarker, M., Lobito, A., Jen, M., Martin, D., Straus, S.E., and Lenardo, M.J. (2004). SPOTS: signaling protein oligomeric transduction structures are early mediators of death receptor-induced apoptosis at the plasma membrane. J. Cell Biol. *167*, 735–744.

Strasser, A., Jost, P.J., and Nagata, S. (2009). The many roles of FAS receptor signaling in the immune system. Immunity *30*, 180–192.

Straus, S.E., Jaffe, E.S., Puck, J.M., Dale, J.K., Elkon, K.B., Rösen-Wolff, A., Peters, A.M., Sneller, M.C., Hallahan, C.W., Wang, J., et al. (2001). The development of lymphomas in families with autoimmune lymphoproliferative syndrome with germline Fas mutations and defective lymphocyte apoptosis. Blood *98*, 194–200.

Walczak, H. (2013). Death receptor-ligand systems in cancer, cell death, and inflammation. Cold Spring Harb. Perspect. Biol. *5*, a008698.

Wang, J., Pielak, R.M., McClintock, M.A., and Chou, J.J. (2009). Solution structure and functional analysis of the influenza B proton channel. Nat. Struct. Mol. Biol. *16*, 1267–1271.

Wang, L., Yang, J.K., Kabaleeswaran, V., Rice, A.J., Cruz, A.C., Park, A.Y., Yin, Q., Damko, E., Jang, S.B., Raunser, S., et al. (2010). The Fas-FADD death domain complex structure reveals the basis of DISC assembly and disease mutations. Nat. Struct. Mol. Biol. *17*, 1324–1329.

Wu, H., and Hymowitz, S.G. (2009). Structure and function of tumor necrosis factor (TNF) at the cell surface. In Handbook of cell signaling, R.A. Bradshaw and E.A. Dennis, eds. (Oxford: Academic Press), pp. 265–275.

Wu, B., Peisley, A., Tetrault, D., Li, Z., Egelman, E.H., Magor, K.E., Walz, T., Penczek, P.A., and Hur, S. (2014). Molecular imprinting as a signal-activation mechanism of the viral RNA sensor RIG-I. Mol. Cell *55*, 511–523.

Zhu, J., Luo, B.H., Barth, P., Schonbrun, J., Baker, D., and Springer, T.A. (2009). The structure of a receptor with two associating transmembrane domains on the cell surface: integrin alphaIIbbeta3. Mol. Cell *34*, 234–249.

Molecular Cell, Volume *61*

Supplemental Information

Structural Basis and Functional Role of Intramembrane Trimerization of the Fas/CD95 Death Receptor

Qingshan Fu, Tian-Min Fu, Anthony C. Cruz, Prabuddha Sengupta, Stacy K. Thomas, Shuqing Wang, Richard M. Siegel, Hao Wu, and James J. Chou

Supplemental Figures

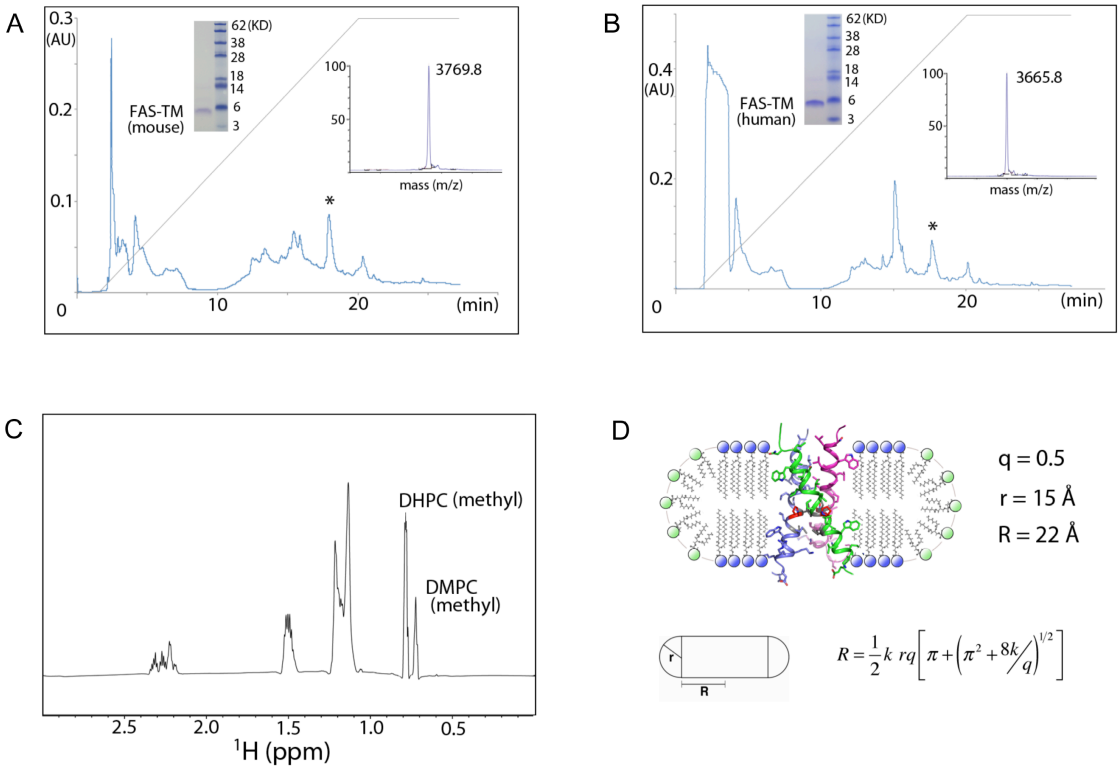

Figure S1. Purification and Reconstitution of Fas-TM Domains (related to Figure 1)

(A) Reverse phase HPLC purification of mouse Fas-TM from CNBr-cleaved trpLE-Fas-TM on Zorbax SB-C3 column with a gradient from 0 – 50% acetonitrile in 5% isopropanol and 0.1% TFA. The product was verified by SDS-PAGE and Mass Spectrometry.

(B) The same as in (A) but for purifying the human Fas-TM.

(C) The 1D ^{1}H NMR spectrum of a reconstituted Fas-TM sample in bicelle at 600 MHz showing the molar ratio of DMPC to DHPC to be ~ 0.5.

(D) An illustration of Fas-TM trimer in bicelle showing the relative sizes of Fas-TM trimer and the q = 0.5 bicelle.

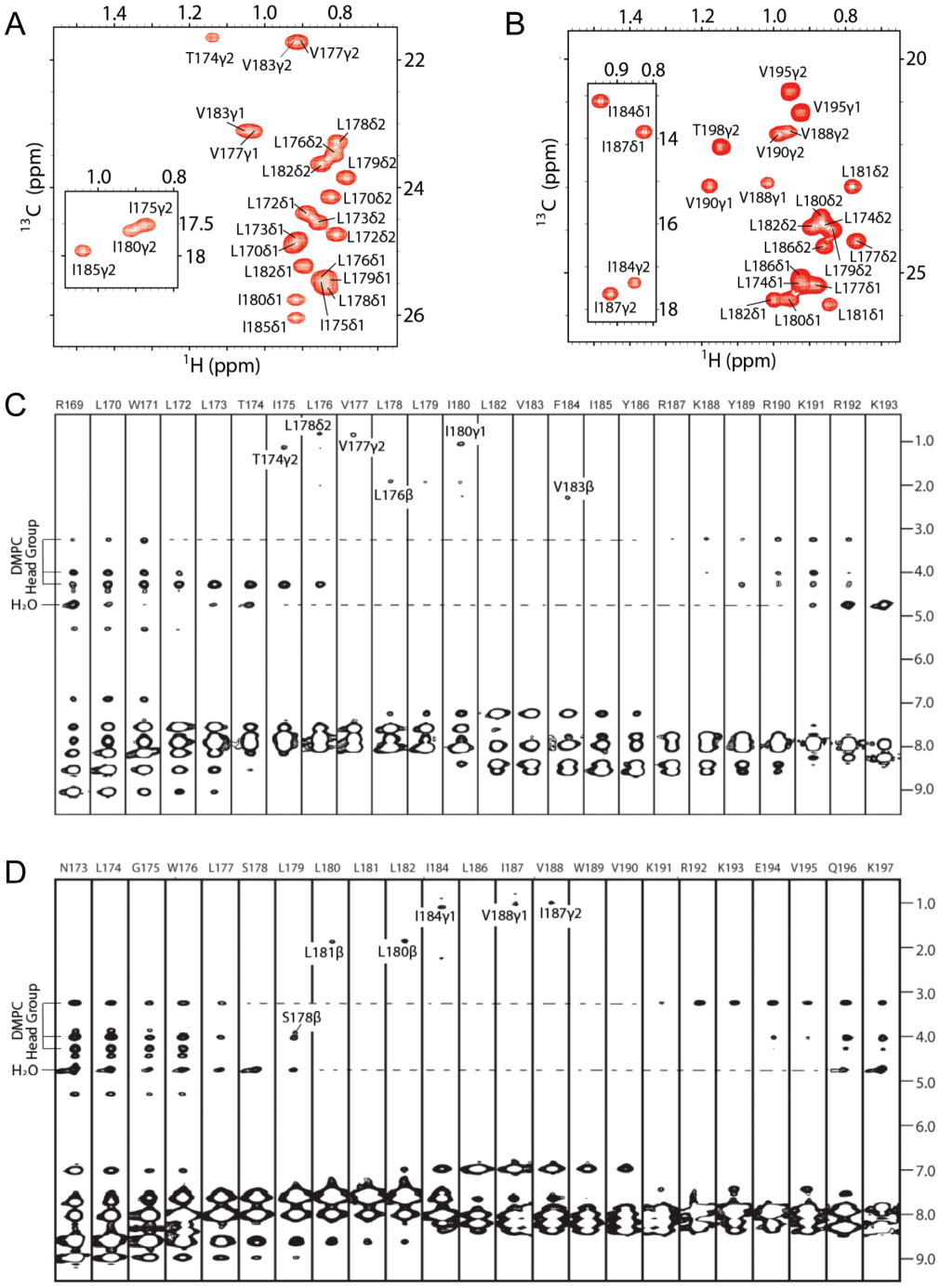

Figure S2. NMR Spectra of Mouse and Human Fas-TM Trimers in Bicelles (related to Figure 2)

(A) The 2D ^{1}H-^{13}C HSQC (28 mM constant time) recorded at 800 MHz showing the assignments of methyl group resonances of the mouse Fas-TM trimer in bicelles.
(B) The same spectrum as in (A) for the human Fas-TM trimer in bicelles.
(C) Residue-specific strips taken from the 3D ^{15}N-separated NOESY-TROSY-HSQC spectrum (NOE mixing time = 300 ms) recorded at 800 MHz using the mouse Fas-TM sample containing 50% (^{15}N, ^{2}H)-labeled peptide and 50% (15% ^{13}C)-labeled peptide. The crosspeaks in the aliphatic regions are intermonomer NOEs between the backbone amide and the sidechain methyl protons.
(D) The same as in (C) showing intermonomer NOEs for the human Fas-TM trimer in bicelles.

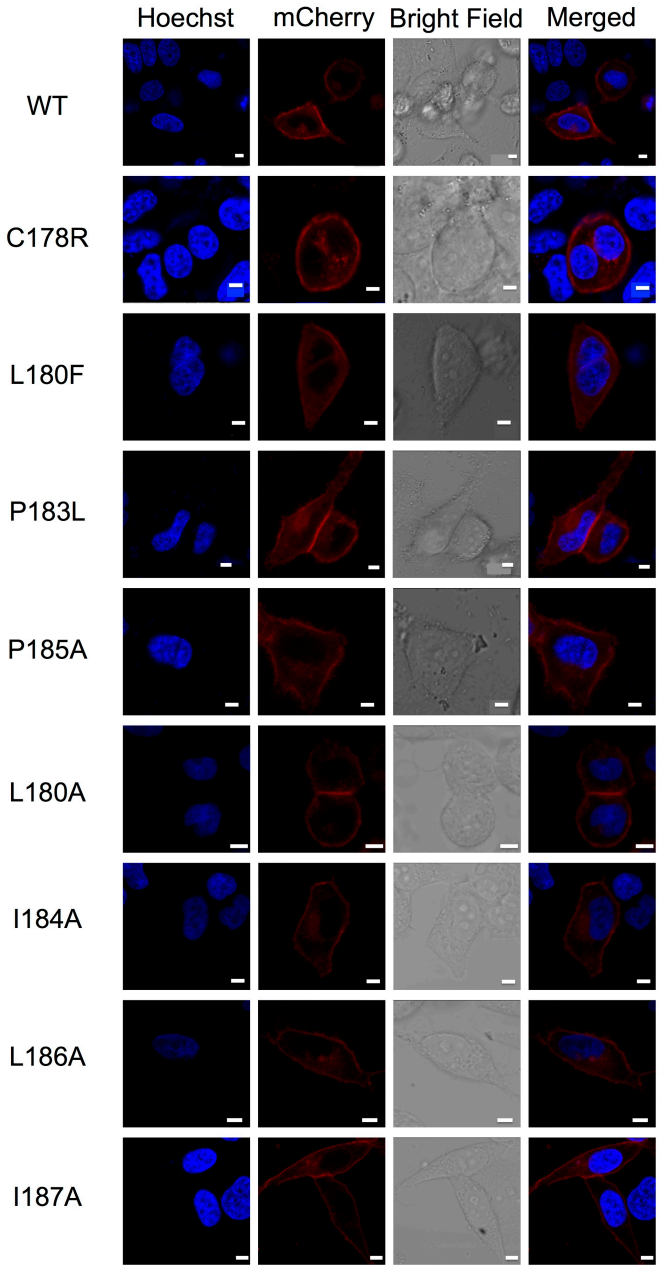

Figure S3. WT and Mutant Fas Proteins were Localized on Plasma Membrane (related to Figure 5)

The WT and mutant Fas-mCherry overexpressed HeLa cells were imaged using fluorescence microscopy. Scale bars, 5 μm.

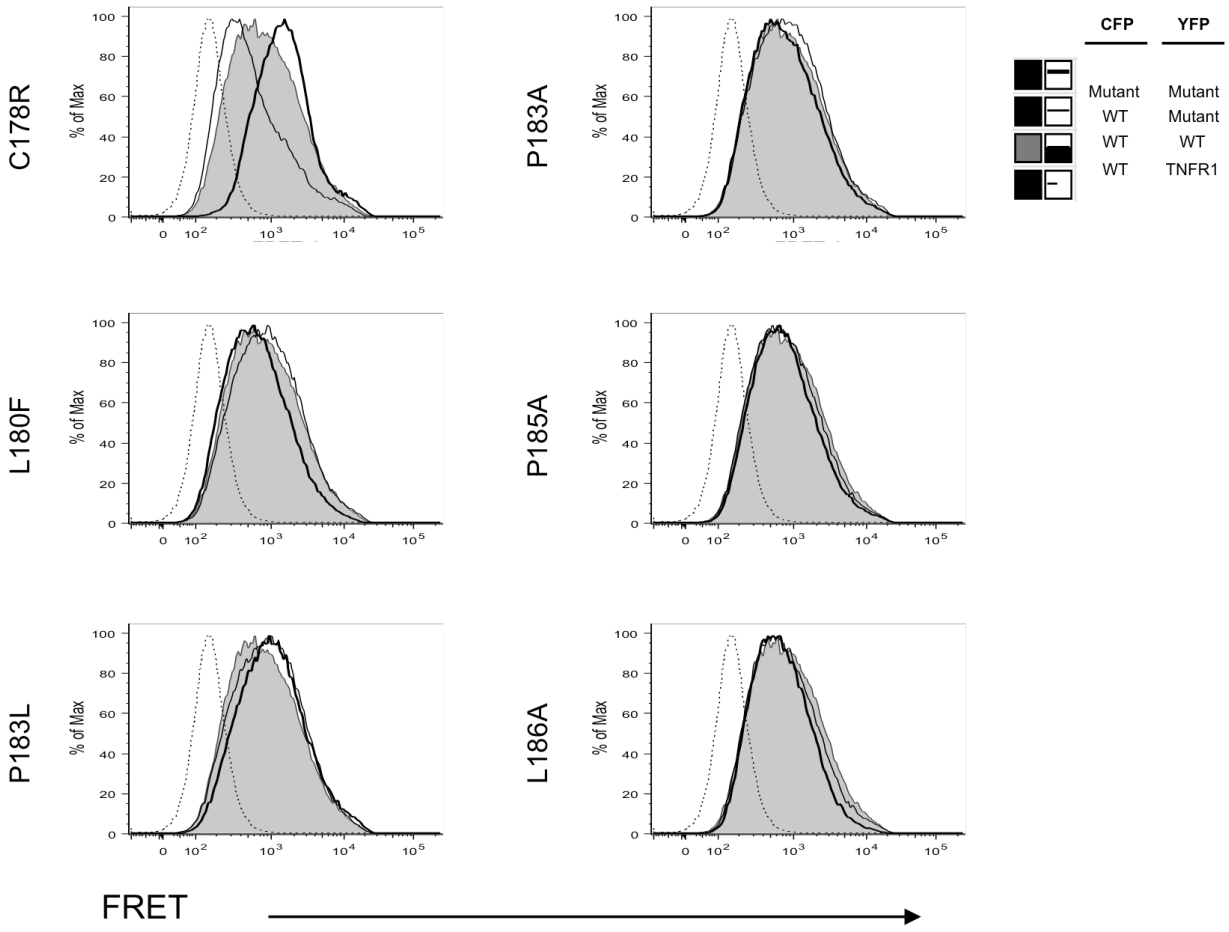

Figure S4: Example Histograms of FRET between Fas transmembrane Mutants (related to Figure 6)

The indicated Fas CFP and YFP fusion proteins and a control TNFR1 fusion protein were cotransfected into 293T cells and FRET assayed by collecting Flourescence in the YFP channel after excitation of CFP by flow cytometry. Histograms of FRET are shown for cells gated to express comparable levels of CFP and YFP.

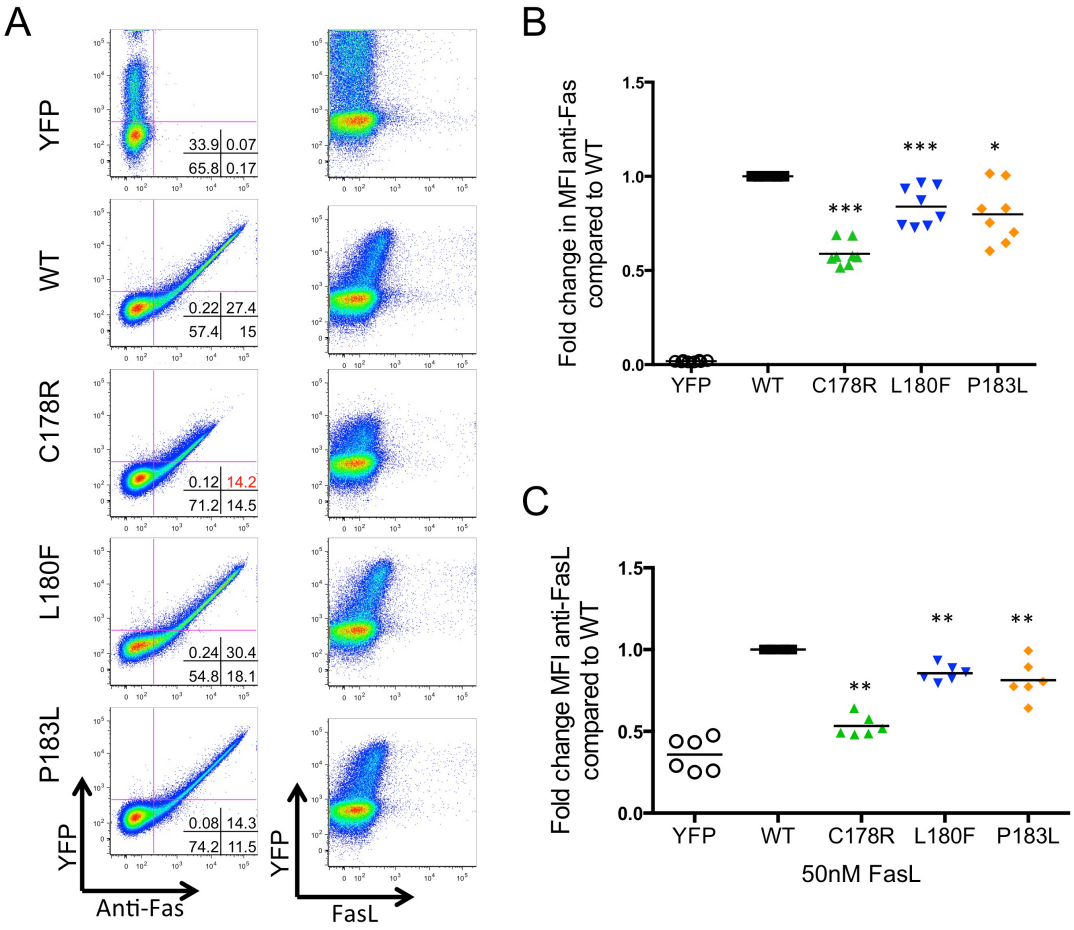

Figure S5. Expression of TM Mutant Fas Proteins on the Plasma Membrane (related to Figure 6)

(A) Representative plots of flow cytometric detection of Fas surface expression and FasL binding of RapoC2 Fas deficient Jurkat cells transfected with the indicated Fas-YFP fusion protein constructs.

(B, C) Relative efficiency of surface Fas (n=8 from 3 experiments) (B) and FasL binding (C) on gated YFP positive RapoC2 cells (n=6 from 2 experiments). * = $p<0.05$, ** = $p<0.005$, *** = $p<0.0005$ by Mann-Whitney test compared to the average of WT Fas expression in each experiment. MFI: mean fluorescence intensity.

Table S1. Relative Intensities of Monomer, Dimer, and Trimer Bands in SDS-PAGE Analyses of Assembly Stability of Fas-TM and Mutants[a, b] (related to Figures 3 and 4)

Mouse Fas-TM mutations [c]

(%)	WT	T174A	T174R	V177A	I180V	I180A	P181A	L182A	V183A
Trimer	88.3±4.6	82.6±5.7	8.0±3.1	84.2±8.7	83.5±6.5	9.7±3.3	5.4±3.0	86.5±7.4	5.3±2.5
Dimer	2.9±1.2	3.0±1.8	21.5±8.6	3.2±1.9	3.2±2.7	12.1±5.1	12.2±3.5	5.0±3.0	10.8±3.8
Monomer	8.8±3.5	14.4±4.2	70.5±9.2	12.6±3.9	13.3±3.2	78.2±8.2	82.4±7.2	8.5±5.8	83.9±5.4

Human Fas-TM mutations [d]

(%)	WT	C178R	L180F	P183L	I184V	I184A	P185A	L186A	I187A
Trimer	85.2±6.9	6.0±3.2	18.5±4.2	8.1±2.3	82.5±6.4	7.4±5.6	11.1±2.3	83.5±6.2	11.0±4.3
Dimer	3.8±2.5	4.8±2.9	6.0±3.3	5.6±1.9	4.2±3.2	30.2±4.3	6.4±3.6	3.6±3.0	23.4±5.2
Monomer	11.0±6.1	89.2±5.0	75.5±7.9	86.3±5.8	13.3±4.1	62.4±5.5	82.5±5.4	12.9±4.8	65.6±7.8

Human Fas-TM Proline 183 mutations and recover mutations [e]

(%)	WT	P183L	P183A	P183L+L181V	P183L+I187V	P183L+L181V+I187V
Trimer	86.0±6.2	5.9±2.3	5.0±2.8	28.1±6.2	25.6±5.2	75.3±5.7
Dimer	4.1±3.1	10.5±4.3	12.1±4.9	9.8±3.7	9.9±4.1	10.4±2.9
Monomer	9.9±4.8	83.6±6.5	82.9±5.3	62.1±5.9	64.5±6.4	14.3±3.6

[a] Gel band intensity is quantified using the program IMAGEJ-V1.49 (Girish and Vijayalakshmi, 2004).

[b] The band intensity is shown as mean ± SD calculated from 3 independent experiments.

[c] Band intensities from SDS-PAGE shown in Figure 3B

[d] Band intensities from SDS-PAGE shown in Figure 3D

[e] Band intensities from SDS-PAGE shown in Figure 4C

Table S2. Comparison of Single Point Energies of Different Fas-TM Mutants[a] (related to Figure 4)

Human Fas-TM

	WT	P183L	P183L+L181V+I197V
Single point energy (KJ/mol)	-4246.287	-3981.197	-4554.752

Mouse Fas-TM

	WT	V177L+V183I	V177L+V183I+L179P
Single point energy (KJ/mol)	-4314.373	-3691.133	-4227.557

[a] The single point energies were computed using the software Schrodinger MacroModel, with the imbedded OPLS_2005 Force field. The dielectric constant was set to 1.0 for electrostatic treatment. The limitations of Van der Waals and short-range electrostatic interactions were smoothly truncated at 7.0 Å and 12 Å, respectively. The protein backbones were restricted with force constant 100 kJ/mol $Å^2$. The side chains were allowed to move freely.

Supplemental Experimental Procedures

Protein Expression and Purification

The human and mouse Fas-TMs were expressed as a C-terminal in-frame fusion to the trpLE sequence with an N-terminal 9-His tag in the pMM-LR6 vector. Transformed *E. coli* BL21 (DE3) cells were spread on a LB-Agar plate and single colony was picked and inoculated into 1 ml LB medium. The overnight-cultured cells were spun down and inoculated into 1000 ml M9 minimal medium with one or more stable isotope labels in 2.0 L baffled flasks. Cultures were grown at 37 °C to O.D. ~0.6 at 600 nm and were induced overnight at 18 °C using 0.1 mM IPTG. Full deuteration of the peptide required growth in 99.9% D_2O with deuterated glucose (Cambridge Isotope Laboratories).

For purification, inclusion bodies were collected by centrifugation at 8000 g after cell lysis by sonication, and were suspended in 6 M guanidine HCl, 50 mM Tris (pH 8.0), 100 mM NaCl, and 1% (v/v) Triton X-100. The fusion protein in the cleared inclusion-body suspension was batch-purified in 8 M urea solution using nickel affinity resins (Sigma-Aldrich). The nickel resins were washed with water and the fusion proteins were eluted with 70% (v/v) formic acid. The FAS-TM peptides were then released from the fusion protein by cleavage at the methionine position by cyanogen bromide (0.1 g/ml) in 70% (v/v) formic acid. The reaction mixture was dialyzed in water, lyophilized and loaded onto a Zorbax SB-C3 column (Agilent) in 90% (v/v) formic acid. Polypeptide fragments were separated using a gradient from 5% (v/v) isopropanol with 0.1% (v/v) trifluoroacetic acid to 50% (v/v) acetonitrile with 5% (v/v) isopropanol and 0.1% (v/v) trifluoroacetic acid. The fractions corresponding to pure FAS-TM peptide were identified by MALDI-TOF mass spectrometry and SDS-PAGE analysis.

Protein Reconstitution Into Bicelles

Lyophilized Fas-TM peptide (1-2 mg) was dissolved in hexafluoro-isopropanal (HFIP) with approximately 9 mg DMPC (protonated or deuterated), followed by drying of the solution under a nitrogen stream to achieve a thin film. The thin films were then dissolved in 3 ml of an 8 M

urea solution containing approximately 27 mg DHPC (protonated or deuterated), followed by dialysis against 20 mM sodium phosphate buffer (pH 6.8) to remove the denaturant. After dialysis, DHPC was added to adjust the ratio of DMPC:DHPC to approximately 1:2. The solution with reconstituted Fas-TM was concentrated using centricon. The final NMR sample contains ~ 1 mM Fas-TM (monomer), 60 mM DMPC, 120 mM DHPC, 20 mM sodium phosphate (pH 6.8), and 5% D_2O. The final DMPC/DHPC ratio was determined using ^{1}H NMR spectrum (Figure S1C).

NMR Spectroscopy

All NMR spectra were collected at 30 °C on Bruker spectrometers operating at ^{1}H frequency of 600 MHz or 800 MHz and equipped with cryogenic probes. The triple resonance and NOE experiments were recorded on Bruker spectrometers operating at 600 and 800 MHz, respectively. Sequence specific assignment of backbone chemical shifts was accomplished using 3 pairs of TROSY-enhanced triple resonance experiments (Salzmann et al., 1999), recorded using a (^{15}N, ^{13}C, ^{2}H)-labeled sample. The triple resonance experiments included HNCA, HN(CO)CA, HN(CA)CO, and HNCO. Protein side chain aliphatic and aromatic resonances were assigned using a combination of NOESYs including ^{15}N-separated NOESY-TROSY-HSQC (150 ms NOE mixing time, τ_{NOE}) and ^{13}C-separated NOESY-HSQC (τ_{NOE} =120 ms). Specific stereo assignment of the methyl groups of valines and leucines were obtained from a 28 ms constant-time ^{1}H-^{13}C HSQC spectrum recorded using a 15% ^{13}C-labeled sample (Szyperski et al., 1992).

The above ^{15}N-separated NOESY-TROSY-HSQC and ^{13}C-separated NOESY-HSQC with short τ_{NOE} were used to assign local NOEs. The combination of local NOE restraints and backbone dihedral angles derived from chemical shifts accurately defined the helical region of the monomer. Intermonomer NOEs between protein backbone amide and side chain aliphatic protons were assigned using a sample that was reconstituted with a 1:1 mixture of (^{15}N, ^{2}H)-labeled and (15% ^{13}C)-labeled peptides. In this sample, the DMPC in the bicelles was also deuterated at the acyl chains. Recording a 3D ^{15}N-separated NOESY-TROSY-HSQC (τ_{NOE} =

300 ms) with this sample allowed exclusive detection of NOE crosspeaks between the ^{15}N-attached protons of one monomer and aliphatic protons of other monomers. The non-deuterated peptide was (15% ^{13}C)-labeled for recording the ^{1}H-^{13}C HSQC spectrum as internal aliphatic proton chemical shift reference while providing stereospecific assignment of leucine and valine methyl groups (Szyperski et al., 1992).

The NMRPipe (Delaglio et al., 1995) and XEASY (Bartels et al., 1995) software were used for data processing and spectral analysis, respectively. TALOS+ was used for predicting backbone dihedral angles from chemical shifts (Shen et al., 2009).

Structure Calculation

Structures were calculated using the program XPLOR-NIH (Schwieters et al., 2003). The monomer structure was first derived in XPLOR-NIH using intramonomer NOE-derived local distances and backbone dihedral restraints derived from chemical shifts using the TALOS+ program (Shen et al., 2009). A total of 10 monomer structures were calculated using a standard simulated annealing (SA) protocol. Three copies of the lowest-energy monomer structure were used to construct an initial model of the trimer using intermonomer NOE restraints collected from the mixed-labeled sample. For each intermonomer restraint between two adjacent monomers, three identical distance restraints were assigned respectively to all pairs of neighboring monomers to satisfy the condition of C3 rotational symmetry. Then, using a SA protocol in which the bath was cooled from 1000 to 20 K, the trimer was refined against the complete set of NOE restraints (including intramonomer and intermonomer distance restraints) and dihedral restraints. The NOE restraints were enforced by flat-well harmonic potentials, with the force constant ramped from 25 to 50 kcal/mol Å^{-2} during annealing. For the defined helical regions, backbone dihedral angle restraints (Φ = -60°, Ψ = -40°) were applied, all with a flat-well (±10°) harmonic potential with force constant ramped from 15 to 30 kcal/mol rad^{-2}. A total of 75 structures were calculated and 15 low energy structures were selected as the structural ensemble. Ramachandran plot statistics for the structure ensemble, calculated using PROCHECK (Laskowski et al., 1993), are as follows: most favored (92.8% for mouse

Fas-TM and 91% for human Fas-TM), additionally allowed (5.4% for both mouse and human Fas-TM), generously allowed (1.8% for mouse Fas-TM and 3.6% for human Fas-TM) and disallowed (0.0% for both mouse and human Fas-TM).

Cell Death Assays

Hela cells were transfected with different plasmids using lipofectamine 2000 according to the standard protocol. Then, cells were harvested and stained by Annexin V-FITC and propidium iodide (PI). The cell counting was carried out using Cellometer (Nexcelom Bioscience) and data was processed through FCS Express 4 software. Both apoptotic and necrotic cells were treated as dead cells. For Fas ligand induced cell death assays, 8 x 10^6 cells were transfected with 25 µg of plasmid DNA expressing full-length Fas (either WT or harboring a TM mutation) via electroporation (BTX ECM 830, Harvard Apparatus). 24 hr post-transfection, cells were purified via Ficoll isolation prior to incubation with increasing levels of isoleucine-zipper fused FasL (FasL-LZ) for 16-18 hr, 37 °C. YFP-positive cells were analyzed for cell death using annexin-V and Live/Dead stain as previously described (Ramaswamy et al., 2011). For experiments testing the dominant inhibitory ability of the TM mutants, Rapo C2 cells were co-transfected with a WT full-length Fas construct fused to ECFP and truncated Fas construct lacking the death-domain (ΔDD, amino acids 211-317) fused to EYFP, either WT or harboring a TM mutation as described above, and transfected cells were stimulated with graded amounts of FasL for 18 hr and apoptosis assayed as above. Specific cell death was calculated as previously described (Ramaswamy et al., 2011) and statistical comparisons were made with a two tailed t-test or Mann-Whitney non-parametric statistics when $n < 9$ or the data did not appear to be normally distributed (Prism 6, Graphpad software).

Supplemental References

Bartels, C., Xia, T.H., Billeter, M., Guntert, P., and Wuthrich, K. (1995). The program XEASY for computer-supported NMR spectral analysis of biological macromolecules. J Biomol NMR *6*, 1-10.

Delaglio, F., Grzesiek, S., Vuister, G.W., Zhu, G., Pfeifer, J., and Bax, A. (1995). NMRPipe: a multidimensional spectral processing system based on UNIX pipes. J Biomol NMR *6*, 277-293.

Girish, V., and Vijayalakshmi, A. (2004). Affordable image analysis using NIH Image/ImageJ. Indian J Cancer *41*, 47.

Laskowski, R.A., MacArthur, M.W., Moss, D.S., and Thornton, J.W. (1993). PROCHECK: a program to check the stereochemical quality of protein structures. J. Appl. Cryst. *26*, 283-291.

Ramaswamy, M., Cruz, A.C., Cleland, S.Y., Deng, M., Price, S., Rao, V.K., and Siegel, R.M. (2011). Specific elimination of effector memory CD4+ T cells due to enhanced Fas signaling complex formation and association with lipid raft microdomains. Cell Death & Differentiation *18*, 712-720.

Salzmann, M., Wider, G., Pervushin, K., and Wuthrich, K. (1999). Improved sensitivity and coherence selection for [15N,1H]-TROSY elements in triple resonance experiments. J Biomol NMR *15*, 181-184.

Schwieters, C.D., Kuszewski, J.J., Tjandra, N., and Clore, G.M. (2003). The Xplor-NIH NMR molecular structure determination package. J Magn Reson *160*, 65-73.

Shen, Y., Delaglio, F., Cornilescu, G., and Bax, A. (2009). TALOS+: a hybrid method for predicting protein backbone torsion angles from NMR chemical shifts. J Biomol NMR *44*, 213-223.

Szyperski, T., Neri, D., Leiting, B., Otting, G., and Wuthrich, K. (1992). Support of 1H NMR assignments in proteins by biosynthetically directed fractional 13C-labeling. J Biomol NMR *2*, 323-334.